



HAL
open science

Pre-salt to salt stratigraphic architecture in a rift basin: insights from a basin-scale study of the Gulf of Suez (Egypt)

Sébastien Rohais, Aurélien Barrois, Bernard Colletta, Isabelle Moretti

► To cite this version:

Sébastien Rohais, Aurélien Barrois, Bernard Colletta, Isabelle Moretti. Pre-salt to salt stratigraphic architecture in a rift basin: insights from a basin-scale study of the Gulf of Suez (Egypt). *Arabian Journal of Geosciences*, 2016, 9 (4), 10.1007/s12517-016-2327-8 . hal-01338357

HAL Id: hal-01338357

<https://hal.science/hal-01338357>

Submitted on 28 Jun 2016

HAL is a multi-disciplinary open access archive for the deposit and dissemination of scientific research documents, whether they are published or not. The documents may come from teaching and research institutions in France or abroad, or from public or private research centers.

L'archive ouverte pluridisciplinaire **HAL**, est destinée au dépôt et à la diffusion de documents scientifiques de niveau recherche, publiés ou non, émanant des établissements d'enseignement et de recherche français ou étrangers, des laboratoires publics ou privés.

Pre-salt to salt stratigraphic architecture in a rift basin: insights from a basin-scale study of the Gulf of Suez (Egypt)

Sébastien ROHAIS^(1*), Aurélien BARROIS⁽²⁾, Bernard COLLETTA⁽²⁾, Isabelle MORETTI⁽³⁾

(1) IFPEN, Direction Géosciences, 1 et 4 Avenue de Bois-Préau, 92852 Rueil-Malmaison Cedex. France

(2) Beicip-Franlab, 232, Av. Napoléon Bonaparte, 92502 Rueil-Malmaison Cedex. France

(3) ENGIE EPI, Département Exploration et Géosciences, 1 Place Samuel de Champlain, 92930 Paris La Défense Cedex

*e-mail address of corresponding author: sebastien.rohais@ifpen.fr

1. INTRODUCTION

Understanding the geology of extensional basins has a major economic impact as more than a third of the global hydrocarbon resources are hosted in rift basins (Mann et al. 2003). Rift basins have even faced a renewed interest during the 2000's with the increase in quality of seismic data resulting in huge discoveries from some rift systems below the salt along Brazilian and African margins (Martin et al. 2009; O'Reilly et al. 2015).

Additionally, if rifts record generally the initial stage of crustal extension they occurred in a wide diversity of tectonic settings ranging from cratonic to orogenic belts settings. Rift basins have then been studied to address many scientific challenges such as the stretching of the continental lithosphere (e.g. McKenzie 1978; Wernicke 1985; Sleekler 1986; Moretti and Chenet 1987), fault dynamics (e.g. Moretti and Colletta 1987; Colletta et al. 1988; Moustafa 1996; Gawthorpe et al. 1997; Gupta et al. 1998; Cowie et al. 2000; Jackson et al. 2002; Khalil and McClay 2002) and the tectonic, sedimentation and erosion relationship (e.g. Leeder and Gawthorpe 1987; Garfunkel 1988; Montenat et al. 1988; Gawthorpe et al. 1990; Lambiase

1 and Bosworth 1995; Bosence et al. 1998; Bosworth et al. 1998; Gupta et al. 1999; Rohais et
2 al. 2007a; Omran and Sharawy 2014). Since the 80's and the recognition of the key role of
3
4 surficial extensional structures and the deeper mantle thermal state, many scientific works
5
6 were addressed to understand the relationship between the subsidence, or more generally the
7
8 vertical movements, and the extension during the rift phases. The initial model of McKenzie
9
10 (1978) emphasized the role of lithospheric and crustal thinning and especially the post-rift
11
12 thermal evolution of the upper mantle to qualify the post-rift subsidence. This post-rift
13
14 subsidence is slow since it is mainly a thermal readjustment and is controlled by the
15
16 conductivity of the mantle. At that time, discussions were still ongoing on the possibility of
17
18 having fast crustal thinning induced by deep thermal anomaly or by far field extensional
19
20 stresses (active versus passive rifting debate). It has then been proven that the crustal and
21
22 lithospheric thinning can be fast enough to fit with the data which show extension may
23
24 happen in just a few millions of years by taking into account a realistic rheology for the
25
26 mantle and crustal rock (e.g. Fleitout and Yuen 1984). In these purely active rifting models,
27
28 the crustal extension is only due to the deep thermal asthenosphere anomaly however the far
29
30 field stresses, that could be or not extensive, influence the resulting rift geometry as proposed
31
32 by Moretti and Froidevaux (1986). The difference between the amount of upper crustal
33
34 extension (Ext_c) and crustal thinning (β_c) has also been recognized for a long time, since deep
35
36 seismic profiles have been acquired. β_c is always bigger than Ext_c and this difference was
37
38 classically interpreted by the authors, in the active rift scheme, in term of different rheologies:
39
40 brittle upper crust and ductile lower crust (Moretti and Pinet, 1987). However, based also on
41
42 the first deep seismic acquisitions, it has been noticed that the localization of the maximum of
43
44 the crustal thinning may not correspond to the maximum of extension in the upper crust and
45
46 proposed crustal-scale fault (i.e. rather brittle lower crust, Wernicke 1985). Meanwhile, data
47
48 from basins where the subsidence is huge compare to the upper crustal extension suggested
49
50
51
52
53
54
55
56
57
58
59
60
61
62
63
64
65

1 that gravity anomalies induced by phase change in the lower crust may also induce subsidence
2 without any far field extension or mantle thermal anomaly (Sleep et al., 1980; Artyushkov
3 and Baer, 1984). Later the works of Huysman (1999) have proven that the “future” of any
4 passive rift is an active one since the destabilization of the lithosphere/asthenosphere
5 boundary is sufficient to start a mantle convective cell that will speed up the lithospheric
6 thinning. The common characteristic of all these proposals to explain rifting, which are not
7 contradictory as all extensional areas have not necessarily the same origin, is that they neglect
8 the effect of the surface processes on the rift evolution. The recognition of the coupling
9 between erosion/sedimentation and deep processes has been facilitated for the last 15 years by
10 the improvement of softwares used to model the lithospheric evolution. This improvement
11 now allows us not only to compute isostatic rebound related to erosion or subsidence due to
12 sediment load, but also to quantify how the upper crustal loading/unloading may influence
13 the mantle state (Burov and Poliakov, 2001; Haines et al. 2003; Cloetingh et al. 2012). One
14 of the key objectives at present is establishing the relationship between deep and surface
15 processes; how does subsidence / extension / uplift / erosion interact all along a rift history? A
16 major limitation preventing the implementation and optimization of these numerical models is
17 the lack of a well constrained case study. A better calibration of theoretical concepts to real
18 data observations is essential to deliver applicable results. Synthetic overviews have been
19 proposed for the evolution from rifting (e.g. Chaboureaud et al. 2013; Macgregor 2015) up to
20 oceanic spreading (e.g. Leroy et al. 2012). However, the time step and depositional system
21 description do not provide enough resolution to constrain, at high resolution, the evolution of
22 a full rift system from its initiation to late rift stages.

23 The present contribution proposes a basin-scale study of a rift basin resulting in a geological
24 scenario including its timing, depocenter migration, depositional system evolution and
25 erosion-sedimentation relationship. The Suez rift has been selected to address this topic as it

1 provides a well constrained geological setting with high resolution dating constraints and a
2 large quantity of accessible and diversified data from both outcrop and subsurface. This study
3
4 is focused on the pre-salt to salt series of the Suez rift that correspond to Oligo-miocene syn-
5
6 rift deposits recording the rift initiation to the latest rift phases.
7
8
9

10 11 **2. SUEZ RIFT: GEOLOGIC BACKGROUND AND BASIN SETTING**

12 The Suez rift is the NW–SE-trending branch of the Red Sea rift system (Figure 1), resulting
13
14 from the late Oligocene to early Miocene rifting of the African and Arabian plates (Garfunkel
15
16 and Bartov 1977). It is bounded on both margins by large-scale normal fault zones (fault
17
18 length ~40-80 km, fault throw ~2-6 km). The polarity of the block-bounding faults changes
19
20 along the axis of the rift, dividing the rift into three 50-100 km long tectonic domains
21
22 (Colletta et al. 1988; Patton et al. 1994; Moustafa 1996): (1) the northern Darag basin with
23
24 southwest dips; (2) the Central basin (Belayim province) with northeast dips; (3) the Southern
25
26 basin (Amal-Zeit province) with southwest dips (Figure 1a). In between, two major ca. 20-km
27
28 wide accommodation zones exist (Colletta et al. 1988): the Zaafarana and the Morgan
29
30 accommodation zones (Figure 1a).
31
32
33
34
35
36
37

38 The stratigraphic succession of the Gulf of Suez includes pre-rift and syn-rift successions
39
40 (Figure 1c). The pre-rift succession is presented hereafter as it constitutes the catchment unit
41
42 feeding the syn-rift depositional systems. It comprises a Precambrian Pan-African crystalline
43
44 basement unconformably overlain by a 1-km thick succession of Cambrian to Eocene
45
46 sedimentary rocks that progressively thins toward the south. This sedimentary succession can
47
48 be subdivided into three distinct units (e.g. Moustafa 1976; Garfunkel and Bartov 1977): (1)
49
50 the "Nubia Sandstones" corresponding to several formations which mostly consist of fluvial
51
52 sandstones (Cambrian to Early Cretaceous), (2) a Late Cretaceous mixed carbonate-
53
54
55
56
57
58
59
60
61
62
63
64
65

1 siliciclastic succession and (3) a Paleocene-Eocene carbonate-dominated succession (Figure
2 1c).

3
4 The transition from pre-rift to syn-rift is locally recorded by red bed deposits overlying a
5 major angular unconformity (Figure 1c). They correspond to the Tayiba and Abu Zenima
6 Formations (Figure 1c) that are commonly attributed to the Oligo-Miocene. This date is based
7 on interbedded basaltic flows and/or volcanic material found within these formations, which
8 absolute K-Ar ages span from 21 to 27 Ma (e.g. Montenat et al. 1986; Plaziat et al. 1998).

9 The syn-rift Miocene succession is subdivided into the Gharandal Group consisting of the
10 Nukhul, Rudeis and Kareem Formations, and the Ras Malaab Group consisting of the
11 Belayim, South Gharib and Zeit Formations (e.g. EGPC 1964; Figure 1c, Figure 2). The post-
12 Zeit succession includes the Wardan and Zaafarana Formations (Figure 2), attributed to the
13 Plio-Pleistocene (e.g. Abd El Shafy 1990). The post-Zeit deposits are not presented in this
14 paper as they correspond to post-rift deposits (Figure 1c).

15
16 The Nukhul Formation is Aquitanian-Early Burdigalian in age (e.g. Garfunkel and Bartov,
17 1977; Fawzy and Abdel Aal 1984; Scott and Govean 1985) and is subdivided into a basal
18 Shoab Ali Member and other three time equivalent members: the Ghara, October and
19 Gharamul Members (Saoudi and Khalil 1984, Figure 2). The Nukhul Formation includes
20 sabkha-type evaporites (anhydrite) and shales, marginal to shallow-marine calcareous
21 conglomerates, reefs and platform carbonates, sandstones, marls and deep marine shales (e.g.
22 Ghorab 1964; Hughes et al. 1992).

23
24 The Rudeis Formation is Burdigalian to Early Langhian in age (e.g. Bunter 1980; Smale et al.
25 1988; Hughes et al. 1992) and is generally subdivided into several members that are
26 commonly grouped into a Lower Rudeis and an Upper Rudeis units (EGPC 1964, Figure 2).

27 The boundary between them is defined by a sharp limit and facies change recording a
28 basinward shift (Garfunkel and Bartov 1977). The Rudeis Formation includes widespread,
29
30
31
32
33
34
35
36
37
38
39
40
41
42
43
44
45
46
47
48
49
50
51
52
53
54
55
56
57
58
59
60
61
62
63
64
65

1 offshore marly/shaly deposits with thin sandstone beds (Lower Rudeis) interpreted as turbidite
2 and debris flow deposits and coarse-grained fan-delta conglomerates with interbedded marls
3
4 and siltstones (Upper Rudeis) (Ghorab 1964). The Rudeis Formation also includes shallow
5
6 marine reefal carbonates developed along isolated tilted block crests (Burchette 1987;
7
8 Bosence et al. 1998).
9

10
11 The Kareem Formation is Langhian in age (e.g. Garfunkel and Bartov 1977; Allen et al. 1984)
12
13 and is subdivided into a basal Markha Member (equivalent to Rahmi Member) and an upper
14
15 Shagar Member (EGPC, 1964, Figure 2). The Markha Member mainly includes thin anhydrite
16
17 beds interbedded with shale, marls and carbonates. The Shagar Member includes shallow
18
19 marine carbonates and sandstones to deep-water marls and dark grey shales (Ghorab 1964).
20
21

22
23 The Belayim Formation is Serravallian in age (e.g. Bunter 1980; Scott and Govean 1985) and
24
25 includes four members: the Baba, Sidri, Feiran and Hammam Faraun Members (EGPC 1964).
26
27

28
29 The Belayim Formation consists of alternating halite, anhydrites, siliciclastics and reef
30
31 carbonates composed of red-algae (Nullipore limestone defined by Sellwood and Netherwood
32
33 1984) recording a wide spectrum of depositional environments from lagoonal and shallow
34
35 platform to deep marine (Figure 2).
36
37

38
39 The South Gharib Formation is Serravallian to Tortonian (e.g. Bunter 1980; Scott and Govean
40
41 1985; Smale et al. 1988, Figure 2) and consists of massive halite and thin anhydrite beds
42
43 interbedded with fine-grained sandstones and shales associated to an alternation of restricted
44
45 hypersaline environments with moderately deep to shallow marine environments (Hughes et
46
47 al. 1992; Rouchy et al., 1995).
48
49

50
51 The Zeit Formation is Messinian (e.g. Bunter 1980; Scott and Govean 1985; Zierenberg and
52
53 Shanks 1986; Richardson and Arthur 1988) and consists of halite, gypsum, anhydrite beds
54
55 interbedded with fine-grained sandstones, siltstones and shales associated to shallow marine
56
57
58
59
60
61
62
63
64
65

1 environments that record alternating restricted to open marine conditions (Hughes et al. 1992;
2 Rouchy et al., 1995; Orszag-Sperber et al. 1998).
3
4
5
6

7 **3. DATA AND METHODOLOGY**

8

9 The database used in the present study results from more than thirty years of collaborative
10 projects leaded by the co-authors with industrial and academic partners on the Suez rift
11 (Chenet 1984; Chenet et al. 1984; Le Quellec and Colletta 1985; Moretti and Froidevaux
12 1986; Moretti 1987; Moretti and Pinet, 1987; Moretti and Colletta 1987; Colletta et al. 1988;
13 Piron 2000; Rohais et al. 2007b; Gargani et al. 2008; Barrois et al. 2010; Barrois 2011;
14 Rohais et al. 2015). It has been uploaded with published works including sedimentological
15 outcrop sections (Burchette 1987; Evans, 1990; Moustafa 1993; Krebs et al. 1997; Bosworth
16 et al. 1998; Gupta et al. 1999; Winn et al. 2001; Abdelghany 2002; Gawthorpe et al. 2003;
17 Jackson et al. 2002; Young et al. 2000; 2003), wells (Hagras and Slocki 1982; Saoudi and
18 Khalil 1984; Chowdhary et al. 1986; Gawad et al. 1986; Hagras 1986; Helmy and Zakaria
19 1986; Evans 1988; Hughes et al. 1992; Schütz 1994; Halim et al. 1996; Salah and Alsharhan
20 1997; Bosworth et al. 1998; El Beialy and Ali 2002; Gawthorpe et al. 2003; Khaled et al.
21 2002; El Beialy et al. 2005; Gargani et al. 2008; Abd El-Naby et al. 2010; Omran and El
22 Sharawy 2014), geological maps, cross-section, isopach and structural maps (Garfunkel and
23 Bartov 1977; Hagras and Slocki 1982; Saoudi and Khalil 1984; Le Quellec and Colletta 1985;
24 Helmy and Zakaria 1986; Colletta et al. 1988; Richardson and Arthur 1988; Schütz 1994;
25 Patton et al. 1994; McClay et al. 1998; Bosworth and McClay 2001; Khalil and McClay 2002;
26 Khaled et al. 2002; Peijs et al. 2012) and paleogeographic maps (Hagras and Slocki 1982;
27 Saoudi and Khalil 1984; Richardson and Arthur 1988; Hughes et al. 1992; Schütz 1994; Salah
28 and Alsharhan 1997; Bosworth et al. 1998; Khaled et al. 2002; Gawthorpe et al. 2003; Peijs et
29 al. 2012).
30
31
32
33
34
35
36
37
38
39
40
41
42
43
44
45
46
47
48
49
50
51
52
53
54
55
56
57
58
59
60
61
62
63
64
65

1 The workflow developed hereafter includes firstly a structural map interpretation and
2 synthesis based on new fieldwork and previous published works (Figure 1). Secondly,
3
4 sequence stratigraphic correlation has been carried out using 279 wells and 31
5
6 sedimentological outcrop sections distributed all over the basin (Figure 1). We refer to the
7
8 stratigraphic surfaces based on the published microfossils and data following the synthesis by
9
10 Richardson and Arthur (1988), Hughes et al. (1992) and El Beialy et al. (2005) (Figure 2).
11
12 These surfaces have been correlated all over the basin along several longitudinal and dip cross
13
14 sections (Figure 3). We then calibrated these stratigraphic ages into absolute ages using the
15
16 ICS (2004) stratigraphic chart based on the synthesis by Gradstein et al. (2012) (Figure 2).
17
18 The pioneer work done by Hughes et al. (1992) has also been used to subdivide the
19
20 stratigraphic period at higher resolution than the formation subdivision to be compatible with
21
22 their microfaunal assemblage zones (B1-4, K1-2, R1-5, Nu1-3; Figure 2). We also refer to the
23
24 work by Krebs et al. (1997) and Wescott et al. (1998) for the sequence labeling (Figure 2).
25
26 Thirdly, lithologic maps have been established (Figure 4) using sequence stratigraphic
27
28 correlation and interpreted using constrains from paleoenvironmental data (Hughes et al.
29
30 1992; El Beialy et al. 2005) and previous published maps (Nuhkul Fm: Saoudi and Khalil
31
32 1984; Khaled et al. 2002; Peijs et al. 2012, Rudeis Fm: Hagra and Slocki 1982; Hughes et al.
33
34 1992; Schütz 1994; Bosworth et al. 1998; Gawthorpe et al. 2003; Peijs et al. 2012, Kareem
35
36 Fm: Hughes et al. 1992; Schütz 1994; Salah and Alsharhan 1997; Khaled et al. 2002; Peijs et
37
38 al. 2012, Belayim Fm: Khaled et al. 2002, South Gharib/Zeit Fms: Richardson and Arthur
39
40 1988). To keep the maps readable, we have only highlighted the deepest part of the basin
41
42 using the paleo-bathymetry constrains from Hughes et al. (1992). Three main bathymetric
43
44 ranges were used with: moderately to deep environments (30-100 m in paleo-bathymetry),
45
46 deep environments (100-200 m in paleo-bathymetry) and very deep environments (> 200 m in
47
48 paleo-bathymetry) (Figure 2, Figure 4). As a result, nineteen lithological maps are presented
49
50
51
52
53
54
55
56
57
58
59
60
61
62
63
64
65

1 over an updated structural framework. A step by step structural restoration was beyond the
2 scope of this study. Indeed, structural restoration and backstripping need as inputs some idea
3 of the paleogeography such as sea floor geometry and eroded thicknesses. In a complex area
4 with contrasted reliefs as the Gulf of Suez, the facies and the lateral variations of these facies
5 are the better indicators of these paleogeographies. As a result the 3D restoration cannot be
6 done before the analysis presented here. All the maps are thus shown over the present day
7 structural framework (Figure 4).
8

9
10
11
12
13
14
15
16
17 Fourthly, isopach / depocenter maps have been established (Figure 5) based on wells and
18 outcrop sections as well as the previous published works using in-house 3D geological
19 modeling tools (Barrois et al. 2010; Barrois 2011).
20
21

22
23
24 Finally, mean sediment supply, mean carbonate accumulation rate and mean evaporite
25 accumulation rate were computed from these 3D database (Table 1) using the same
26 methodology proposed by Poag and Sevon (1989), Rouby et al. (2009) and Guillocheau et al.
27 (2012). For each time step, we computed the relative proportion of the lithologies using an
28 automatic image analysis based on the lithologic maps. The six dominant lithologies have
29 then been gathered into groups to be able to compute an accumulation rate for evaporites
30 (anhydrite and halite), carbonates (carbonates and offshore mudstones) and sediment supply
31 form siliciclastic deposits (shales, sandstones, conglomerates). An optimistic, pessimistic and
32 preferred scenario have been established to explore the maximum and minimum development
33 for each group of lithology depending on the drawing and extrapolation on the maps
34 (Evaporites, Carbonates and Siliciclastics; Table 1). The preferred scenario corresponds to the
35 lithologic maps presented in Figure 4. Then we estimated the volume for each group of
36 lithology by modulating these relative proportions to the volume of preserved sediment for
37 each time steps (Table 1). Carbonate volumes have been corrected with a porosity of 10% and
38 siliciclastic volumes with 20% (e.g. Rouby et al. 2009; Guillocheau et al. 2012). A minimum
39
40
41
42
43
44
45
46
47
48
49
50
51
52
53
54
55
56
57
58
59
60
61
62
63
64
65

1 and maximum have also been computed to established error bar on the accumulation rates as
2 well as on the sediment supply (Table 1) and are presented in Figure 6.
3
4
5
6

7 **4. STRATIGRAPHIC ARCHITECTURE AND PALEOGEOGRAPHY**

8

9 Stacking pattern has been used to correlate the main surfaces at basin-scale and then to
10 characterize the distribution of the main syn-rift formations (Figure 2, Figure 3). The
11 identification of the main facies, environment of deposition (EOD) and depositional profiles is
12 based on the solid sedimentological and environmental knowledge provided by previous
13 studies (e.g. Burchette, 1987; Montenat et al. 1988; Gawthorpe et al. 1990; Hughes et al.
14 1992; Rouchy et al. 1995; Salah and Alsharhan 1997; Bosence et al. 1998; Gupta et al. 1999;
15 Young et al. 2000; Winn et al. 2001; Jackson et al. 2005; Abd El-Naby et al. 2010; Omran
16 and El Sharawy 2014; Figure 2). Stratigraphic architecture has then been restored by
17 interpreting the sequences using six dominant lithologies: carbonates (including reef and
18 platform s.l. deposits), shales (silty rich from protected to restricted deposits, versus mud rich
19 for offshore deposits), sandstones (including fan delta, shallow marine and turbiditic
20 deposits), conglomerates (including alluvial fan and fan delta deposits), anhydrite and halite
21 (mainly from lagoon and saline to sabkha depositional settings).
22
23
24
25
26
27
28
29
30
31
32
33
34
35
36
37
38
39
40
41
42

43 *4.1 Nukhul Formation (Miocene, ~Aquitainian, ca. 20.4-23 Ma)*

44

45 The timeframe defined by Hughes et al. (1992) has been used to establish three key phases
46 during the Nukhul Fm deposition (N1 to N3, each of which lasted ca. 0.9 Myr). The main
47 hypothesis for the paleogeographic restoration was that the Shoab Ali Mb was time equivalent
48 to Nukhul Fm deposits in the northern part of the rift, a consistent interpretation with the
49 Bosworth and McClay (2001) review. The Nukhul Fm recorded a progressive flooding from
50 the Mediterranean Sea (Figure 4a-c) with a progressive evolution from supra-littoral to
51
52
53
54
55
56
57
58
59
60
61
62
63
64
65

1 moderately deep depositional environments (paleo-bathymetry 30-100 m). Large scale
2 tectonic structures (e.g. accommodation zone, Darag, Central and Southern basins) as well as
3
4 small scale structures (e.g. tilted block crest, hanging-wall and relay ramp) clearly had an
5
6 influence onto facies distribution and partitioning (Figure 4a-c). The tilted block crests are
7
8 commonly surrounded by shallow carbonate deposits while in the hanging-wall setting
9
10 siliciclastic dominated deposits mainly occurred especially in the Central and Southern basins
11
12 (Figure 4a-c).
13
14
15
16
17
18

19 *Nu3 (ca. 22.1-23Ma)*

20
21 The Darag, Central and Southern basins were individualized in terms of depositional
22
23 environments (Figure 4a). To the south, the Southern basin was characterized by siliciclastic
24
25 dominated deposits with alluvial fan and fluvio-lacustrine depositional environments. The
26
27 Morgan accommodation zone was mainly sub-aerial and starved of sediment (Figure 4a). The
28
29 Central basin was characterized by mixed deposits with shallow marine to restricted deposits.
30
31 The Zaafarana accommodation zone was characterized by shallow marine deposits recording
32
33 the transition toward open marine setting to the north (Figure 4a). The Darag basin was thus
34
35 mainly characterized by open marine deposits (Figure 4a).
36
37
38
39
40
41
42

43 *Nu2 (ca. 21.2-22.1Ma)*

44
45 The Darag, Central basins were still individualized in term of depositional environments from
46
47 the Southern basin showing a N-S depositional gradient (Figure 4b). The marine flooding
48
49 from the Mediterranean Sea reached the Central basin. The input of siliciclastics decreased
50
51 relatively to the south in comparison with Nu3. The depositional profile includes carbonate
52
53 platforms and isolated reefs along tilted block crests and submerged paleohighs facing
54
55 moderate to deep basinal marine shales (Darag and Central basins, Figure 4b). The Southern
56
57
58
59
60
61
62
63
64
65

1 basin was characterized by lagoon deposits and marginal marine sabkha evaporites (Figure
2 4b). There was no clear evidence that the marine flooding originated from the Red Sea to the
3
4 south.
5
6

7 8 9 *Nul (ca. 20.4-21.2Ma)*

10
11 The overall flooding coming from the Mediterranean Sea progressively reached the Morgan
12 accommodation zone (Figure 4c). Deep marine sediments were deposited in the Darag basin
13 (Figure 4c). The input of siliciclastics became progressively localized along the future rift
14 shoulders. Evaporites were preserved in isolated ponds from marginal marine systems in the
15 Southern basin (Figure 4c). There was still no evidence that marine flooding originated from
16 the Red Sea.
17
18
19
20
21
22
23
24
25
26
27

28 29 *4.2 Rudeis Formation (Miocene, ~Burdigalian, ca. 15.8-20.4 Ma)*

30
31 The periods of time defined by Hughes et al. (1992) has been used to establish four key
32 phases during the Rudeis Fm deposition (R5, R3, R2 and R1). The Rudeis Fm recorded the
33 flooding from both the Mediterranean Sea and the Red Sea and their connection (Figure 4d-
34 g). It has recorded the deepest depositional environments (> 200 m in bathymetry) and a least
35 four main anoxic events (Hughes et al. 1992; Figure 2). Large and small scale tectonic
36 structures influenced facies distribution and partitioning (Figure 3). While during the Nukhul
37 Fm deposition the three main basins were characterized by different depositional setting
38 suggesting a N-S paleogeographic gradient, the Rudeis Fm progressively recorded deep open
39 marine condition all along its axis from the Darag to the Southern basin (Figure 4d-g). The
40 Southern basin and Morgan accommodation zone were preferentially fed by siliciclastics in
41 response to the Precambrian basement denudation, while the Darag basin was mainly
42 characterized by carbonate dominated deposits (Figure 4d-g). Siliciclastics sources were
43
44
45
46
47
48
49
50
51
52
53
54
55
56
57
58
59
60
61
62
63
64
65

1 distributed all along the rift bounding faults. Very coarse-grained conglomerate sources were
2 localized on the steep relief located on the eastern side of the rift (Figure 4d-g).
3
4
5

6
7 *R5 (ca. 19.6-20.4Ma)*
8

9 The Rudeis Fm was strongly transgressive onto the Nuhkul Fm with several onlap features
10 indicating a widening of the depocenters (Figure 3). Very deep (200-400 m deep) open marine
11 conditions occurred all along the basin axis with local anoxia (Hughes et al., 1992, Figure 4d).
12 It was the very first time that a marine connection occurred between the Mediterranean Sea
13 and the Red Sea (Figure 4d). The input of siliciclastics was mainly localized along the rift
14 shoulders and most of the tilted block crests were progressively onlapped by carbonate reefs
15 and platforms (Figure 4d). Sandstones were locally delivered to the basin axis throughout the
16 main accommodation zones (Morgan and Zaafarana) and smaller relay ramp areas (e.g. Baba-
17 Belayim area, Figure 4d). The R5 period of time is interpreted as the overall maximum
18 flooding event during the rift evolution (Figure 2).
19
20
21
22
23
24
25
26
27
28
29
30
31
32
33
34
35

36 *R3 (ca. 17.6-18.5 Ma)*
37

38 The trend initiated during the previous stage continued with very deep open marine conditions
39 all along the basin axis and input of siliciclastics along the rift shoulders (Figure 4e). The R3
40 period of time recorded the widest spread and thickest distal offshore deposits (Figure 4e),
41 with very deep (200-400 m deep) open marine conditions characterized by another major
42 anoxic event (Hughes et al., 1992; Figure 2).
43
44
45
46
47
48
49
50
51
52

53 *R2 (ca. 16.7-17.6 Ma)*
54

55 The R2 period of time (equivalent to the basal portion of the Upper Rudeis) marked a major
56 change during the rift evolution (Figure 4f), traditionally related to the mid-Clysmic event
57
58
59
60
61
62
63
64
65

1 (Garfunkel and Bartov 1977). A major increase in the sediment supply from the eastern rift
2 shoulder was recorded by large and very coarse-grained fan deltas (Figure 4f). The basin axis
3
4 also recorded a major pulse in siliciclastics (Figure 4f). The isolated platforms developed
5
6 along tilted block crests were characterized by thickening and widening trends suggesting a
7
8 relative imbalance of production rate over the accommodation space. This could be
9
10 interpreted as a progressive subsidence of the tilted block crests. Short duration anoxic events
11
12 could have locally occurred (Hughes et al. 1992; Figure 2). The R2 period of time marked the
13
14 transition toward an overall forced regressive trend at rift scale that was recorded by the
15
16 Upper Rudeis, Kareem and Belayim Formations (Figure 2).
17
18
19
20
21
22
23

24 *R1 (ca. 15.8-16.7Ma)*

25
26 The forced regressive trend initiated during the previous stage continued (Figure 4g). The R1
27
28 period of time recorded the last major anoxic event during the rift evolution (Hughes et al.
29
30 1992; Figure 2). A progressive decrease in paleo-bathymetry and a change in sea bottom
31
32 conditions have been inferred from the benthonic foraminifera assemblages (Hughes et al.
33
34 1992; Figure 2). The R1 deposits are organized in an overall prograding trend up to the first
35
36 major sequence boundary (T30, boundary between Rudeis and Kareem Formations) recorded
37
38 at basin-scale (e.g. Figure 3d, massive sandstone package organized in a forced regressive
39
40 trend along well 47).
41
42
43
44
45
46
47

48 *4.3 Kareem Formation (Miocene, ~Langhian, ca. 13.6-15.8 Ma)*

49
50 We mainly refer to the work done by Hughes et al. (1992), Salah and Alsharhan (1997) and El
51
52 Beialy et al. (2002) to establish four key phases during the Kareem Fm deposition (Figure 4h-
53
54 k). The Kareem Fm recorded the progressive disconnection between the Mediterranean Sea
55
56 and the Red Sea (Figure 4h-k). Deep to very deep water depositional environments were
57
58
59
60
61
62
63
64
65

1 developed (> 200 m in bathymetry), nevertheless, the Kareem Fm constitutes a transition
2 toward mainly oxic paleoenvironmental conditions (Hughes et al. 1992; Figure 2). Large scale
3 tectonic structures had a major influence onto facies distribution and partitioning (Figure 4h-
4 k). As for the previous period of time (Rudeis Fm), siliciclastics were mainly preserved in the
5 Southern basin, Morgan accommodation zone and along the rift bounding faults.
6
7
8
9
10

11
12
13
14 *K2 – basal Markha (ca. 15.3-15.8 Ma)*
15

16 The K2 – basal Markha deposits overlaid a major sequence boundary (T30 ca. 15.8 Ma;
17 Figure 2, Figure 3). Open marine conditions still prevailed in the northern part of the rift
18 (Darag basin and Zaafarana accommodation zone) and the southernmost part (SE of the
19 Southern basin). Very large carbonate platforms occurred in the Southern basin and along the
20 Zaafarana accommodation zone (Figure 4h). The Central basin was characterized by large and
21 thick anhydrite deposits laterally passing to shallow marine carbonates to the north and to the
22 south east (Figure 4h). This paleogeographic configuration thus recorded the first evidence
23 during the syn-rift deposition of disconnection between the Mediterranean Sea and the Red
24 Sea (Figure 4h). Rift shoulders still constituted the main source areas for siliciclastics (Figure
25 4h).
26
27
28
29
30
31
32
33
34
35
36
37
38
39
40
41
42

43 *K2 – Middle Markha (ca. 14.8-15.3 Ma)*
44

45 The K2 – Middle Markha deposits recorded a new major flooding from both the
46 Mediterranean Sea and the Red Sea (Figure 4i). Depositional environments and lithology
47 distributions were very similar to those occurring during the deposition of the R3-Rudeis Fm
48 deposits with neither evidences of anoxic nor suboxic conditions (Figure 2) as paleo-
49 bathymetry was relatively lower (Figure 4i).
50
51
52
53
54
55
56
57
58
59
60
61
62
63
64
65

K2/K1 transition – Markha/Shagar (ca. 14.3-14.8 Ma)

1
2 The K2/K1 transition – Markha/Shagar deposits recorded another major disconnection
3
4 between the Mediterranean Sea and the Red Sea. As for the K2 – basal Markha deposits, open
5
6 marine conditions only prevailed in the northern part and the southernmost part of the Suez
7
8 rift (Figure 4j). The Zaafarana accommodation zone controlled the occurrence of a large
9
10 carbonate platform recording the transition from open marine setting to the north to a
11
12 restricted setting in the Central basin (Figure 4j).
13
14
15
16
17
18

K1 – Top Shagar (ca. 13.6-14.3 Ma)

19 The K1 – Top Shagar deposits recorded a major flooding event occurring at basin-scale
20
21 (Figure 4k). Isolated platforms were very small and restricted to tilted block crests (Figure
22
23 4k). Siliciclastic were mainly derived from the rift shoulders, especially in the Southern basin
24
25 and along the Morgan accommodation zone (Figure 4k). The topmost part of K1 – Top
26
27 Shagar deposits are organized in an overall prograding trend up to the second major sequence
28
29 boundary recorded at basin-scale (T50 ca. 13.6 Ma; Figure 2, Figure 3).
30
31
32
33
34
35
36
37
38

4.3 Belayim Formation (Miocene, ~Serravallian , ca. 11.8-13.6 Ma)

39 The periods of time defined by Hughes et al. (1992) have been used to establish four key
40
41 phases during the Belayim Fm deposition (B4, B3, B2 and B1). The Belayim Fm recorded a
42
43 progressive disconnection between the Mediterranean Sea and the Red Sea in the Suez rift
44
45 (Figure 4l-o). It has recorded the first thick and widely distributed salt deposits over the Suez
46
47 rift (Figure 3, Figure 4l). The Belayim Fm also illustrates the full depositional profile from
48
49 open marine setting in the south (Southern basin) to restricted environments with a lateral
50
51 facies change from anhydrite to halite in the north (Darag basin, Figure 4l and n). Small scale
52
53 tectonic structures had influence onto facies distribution (e.g. faulted controlled depocenters
54
55
56
57
58
59
60
61
62
63
64
65

1
2
3
4
5
6
7
8
9
10
11
12
13
14
15
16
17
18
19
20
21
22
23
24
25
26
27
28
29
30
31
32
33
34
35
36
37
38
39
40
41
42
43
44
45
46
47
48
49
50
51
52
53
54
55
56
57
58
59
60
61
62
63
64
65

with halite on Figure 4l). The input of siliciclastic was mainly localized along the Morgan accommodation zone and in the Central basin (Figure 4l-o).

B4 – Baba (ca. 13.1-13.6 Ma)

The B4 – Baba deposits recorded the first disconnection of the entire Suez rift from the Mediterranean Sea and an overall restriction of the Darag, Central and Southern basins (Figure 4l). Halite deposits were preserved in fault controlled depocenters (Figure 4l). Sediment supplies along the rift shoulders were very low as suggested by the very small isolated siliciclastics bodies (e.g. Wadi Araba, Belayim and Baba areas; Figure 4l). A large carbonate platform was developed to the south of the Southern basin, recording the transition toward more open marine setting in the Rea Sea to the south (Figure 4l).

B3 – Sidri (ca. 12.6-13.1 Ma)

The B3 – Sidri deposits (as the top Shagar) recorded one of the last flooding events occurring at basin-scale in the Suez rift (Figure 4m). The Southern basin was characterized by a restricted environment along its western part (Zeit area), while open marine conditions prevailed along a north to south corridor to the east (Figure 4m). Siliciclastic supplies were mainly localized in the Central basin and along the Morgan accommodation zone where the Precambrian basement was denudated (Figure 4m).

B2 – Feiran (ca. 12.1-12.6 Ma)

The B3 – Feiran deposits recorded a second full disconnection from the Mediterranean Sea as the B4 – Baba deposits (Figure 4n). Halite deposits were preserved in fault controlled depocenters in the Southern basin and along the Morgan accommodation zone suggesting less intense evaporation processes in the Central basin compared to the B4 – Baba period of time

1
2
3
4
5
6
7
8
9
10
11
12
13
14
15
16
17
18
19
20
21
22
23
24
25
26
27
28
29
30
31
32
33
34
35
36
37
38
39
40
41
42
43
44
45
46
47
48
49
50
51
52
53
54
55
56
57
58
59
60
61
62
63
64
65

(Figure 4l). Very small isolated siliciclastics bodies were preserved especially in the Wadi Araba, Belayim and Baba areas (Figure 4n). As for the B4 – Baba deposits, a large carbonate platform was developed to the south of the Southern basin (Figure 4n).

B1 – Hammam Faraun (ca. 11.8-12.1 Ma)

The B1 – Hammam Faraun deposits recorded the very last marine flooding event occurring at basin-scale connecting the Mediterranean Sea and the Red Sea (Figure 4o). Paleogeographic setting was very similar to the B3 – Sidri period of time, with restricted and shallow environments in the Zeit area and isolated inputs of siliciclastics (Wadi Araba, Morgan Accommodation zone, Belayim and Baba areas; Figure 4o). The restricted depositional environments preserved to the east of the Darag basin and the open marine deposits to the north were the last sedimentary records before a long period of erosion and/or non-deposition to the north of the Suez rift (Figure 4o).

4.4 South Gharib Formation (Miocene, ~Tortonian , ca. 7.2-11.8 Ma)

No high resolution biostratigraphic constraints for the South Gharib Fm were available as the ones provided by Hughes et al. (1992) for the previous formations. We thus choose to highlight only two key phases during the deposition of the South Gharib Fm: its lowermost and uppermost parts. The three main basins were characterized by a north to south paleogeographic gradient with highly evaporitic setting to the south and more siliciclastic and mixed setting to the north (Figure 4p-q). Halite deposits were preserved in fault controlled depocenters (Figure 3, Figure 4p-q). The input of siliciclastic was spatially localized and almost corresponded to the present day feeding points (Figure 4p-q). Evaporation processes were the dominant sedimentary processes.

1
2
3
4
5
6
7
8
9
10
11
12
13
14
15
16
17
18
19
20
21
22
23
24
25
26
27
28
29
30
31
32
33
34
35
36
37
38
39
40
41
42
43
44
45
46
47
48
49
50
51
52
53
54
55
56
57
58
59
60
61
62
63
64
65

Lower South Gharib (ca. 9.5-11.8 Ma)

The Lower South Gharib deposits overlaid a major sequence boundary (T60 ca. 11.8 Ma; Figure 2, Figure 3). For the very first time, anhydrite and halite deposits occupied the whole of the Suez rift (Figure 4p). Fault controlled depocenters characterized by halite deposits were connected into very large depocenters in the Southern basin up to the Morgan accommodation zone (Figure 4p). The Central basin and the Zaafarana accommodation zone were characterized by anhydrite deposits with fault controlled halite deposits, recording the transition toward the Darag basin where only condensed siliciclastic deposits were preserved (Figure 3, Figure 4p). There were no preserved deposits in the northern part of the Darag basin (Figure 3, Figure 4p).

Upper South Gharib (ca. 7.2-9.5 Ma)

The Upper South Gharib deposits were organized in a similar trend as the South Gharib deposits with highly evaporitic setting to the south (Figure 3, Figure 4q). The Southern and Central basins were characterized by fault controlled halite depocenters connected by very continuous anhydrite deposits (Figure 4q). The inputs of siliciclastics were localized along the main feeding points already active during the deposition of the Lower South Gharib (Figure 4q). The size of the fan systems was much larger than during the deposition of the Lower South Gharib suggesting an increase in the water supplies coming from the catchment areas (Figure 4q).

4.5 Zeit Formation (Miocene, ~Messinian , ca. 5.3-7.2 Ma)

As it happens for the case of the South Gharib Fm, no high resolution biostratigraphy was available for the Zeit Fm so it was subdivided into a lower and an upper part (Figure 4r-s).

The same paleogeographic gradient as for the South Gharib Fm deposition was identified with

1 highly evaporitic setting to the south (Figure 3, Figure 4r-s). Halite and/or anhydrite deposits
2 were preserved in fault controlled depocenters (Figure 4r-s). The input of siliciclastic was
3 spatially localized and almost corresponds to the present day feeding points (Figure 4r-s).
4
5 Evaporation processes were still important, but the input of siliciclastics increased as well as
6
7 mixed carbonate dominated deposits compared to the South Gharib period of time suggesting
8
9 more humid climatic setting (Figure 3, Figure 4r-s).
10
11
12
13
14
15
16

17 *Lower Zeit (ca. 6.2-7.2 Ma)*

18
19 The Lower Zeit deposits recorded a period of relatively low occurrence of evaporate deposits
20 during the Tortonian-Messinian time interval (Figure 4r). Small isolated evaporitic
21
22 depocenters occurred in the Central and Darag basins mainly filled with anhydrite and few
23
24 halite deposits (Figure 4r). The Southern basin was characterized by fault controlled halite
25
26 small depocenters connected by very continuous anhydrite deposits (Figure 4r). Siliciclastic
27
28 supplies were the highest during the Tortonian-Messinian time interval (Figure 6). There were
29
30 no deposits preserved in the northern part of the Darag basin (Figure 3, Figure 4r).
31
32
33
34
35
36
37
38

39 *Upper Zeit (ca. 6.2-5.3 Ma)*

40
41 The Upper Zeit deposits recorded another pulse in evaporitic conditions, almost equivalent to
42
43 the Upper South Gharib Fm in term of spatial distribution (Figure 4s). Two large fault
44
45 controlled depocenters with halite were preserved in the Central basin. The Southern basin
46
47 was still characterized by small fault controlled depocenters with halite and continuous
48
49 anhydrite deposits (Figure 4s). Siliciclastic supplies were still high with large localized fan
50
51 system (Figure 4s). No deposits from this age were preserved in the northern part of the Suez
52
53
54
55
56
57
58
59
60
61
62
63
64
65

5. RIFT DYNAMICS, SUBSIDENCE AND UPLIFT

1
2 The presented stratigraphic architecture restoration (Figure 3, Figure 4) has been then
3
4 combined to thickness and depocenter maps analysis (Figure 5) and discussed in the light of
5
6 the subsidence and uplift dynamics within the rift evolution taking into account the published
7
8 subsidence analysis (Steckler 1985; Moretti and Colletta 1987; Moretti and Chenet 1987;
9
10 Richardson and Arthur 1988; Figure 6). The total amount of uplift/exhumation during the rift
11
12 evolution has been estimated to about 5-7 km on the western rift shoulder (Omar et al. 1989).
13
14
15
16
17
18

5.1 Rift initiation (Oligocene, ~Chattian. ca. 1-4Myr duration)

19
20 Faunas, stratigraphic relationships, K-Ar and Ar-Ar dates indicate that the onset of the rifting
21
22 is no younger than 25-27 Ma in the Southern basin area (e.g. El Shinnawi 1975; Purser and
23
24 Hötzl 1988), 23-25 Ma for the Central basin area (e.g. Plaziat et al. 1998) and ca. 23.5 Ma for
25
26 the Darag basin and the Cairo-Suez areas (Kappelman et al. 1992; Lotfy et al. 1995)
27
28 suggesting a rift propagation toward the north that is consistent with recent observation from
29
30 the Nile delta (Sarhan et al. 2014).
31
32
33
34
35

36 Two preserved depocenters 50-60 km wide are localized over the future main Southern and
37
38 Central domains of the Suez rift (Figure 5a). To the North, there is no data from the Darag
39
40 basin depocenter to illustrate Oligocene deposits but only few witnesses in the northernmost
41
42 part of the Suez rift (Figure 5a). The central part is also characterized by volcanism along the
43
44 rift shoulders and rift axis (Figure 5a). Basaltic dikes, sills and flows have sub-alkaline to
45
46 alkaline affinities and have been interpreted to be diagnostic of intraplate, tensional
47
48 environment (Moussa 1987).
49
50
51
52

53 Subsidence was very low during the Late Oligocene (Steckler 1985; Moretti and Colletta
54
55 1987; Richardson and Arthur 1988) and reliefs mainly corresponded to inherited topography
56
57 from the Syrian Arc such as the Wadi Araba structure (Garfunkel 1988; Evans 1990; Khaled
58
59
60
61
62
63
64
65

1 et al. 2002; Figure 1). Basement was already exposed to the South (present day Red Sea) by
2 late Oligocene times (Thiriet 1987). The onset of rift-related uplift in Sinai has been proposed
3 around 26.6 +/- 3 Myr based on Fission Track Analysis (Kohn and Eyal 1981).
4
5
6
7
8

9 *5.2 Rift widening (Miocene, ~Aquitainian, ca. 3Myr duration)*

10 The presence of growth-strata in the Nukhul Fm indicates that extensional faults were active
11 during the Aquitainian (e.g. Colletta et al 1988; Jackson et al. 2002). The rift was subdivided
12 into numerous depocenters (Figure 5b) controlled by active faults recording a progressive
13 fault linkage and interaction (e.g. Leeder and Gawthorpe 1987; Gawthorpe et al. 1997; Khalil
14 and McClay 2002; Jackson et al. 2002). Meanwhile, some former faults were abandoned. This
15 first major phase of extension was characterized by a low tectonic subsidence (0-100m/Myr,
16 Moretti and Colletta 1987; Richardson and Arthur 1988). The Nubia Sandstones and the
17 crystalline basement were the main feeding sources for sediment delivery into the Southern
18 basin. Scarce boulder conglomerates and breccias suggest high local relief in the Central basin
19 as well as in the Southern basin (e.g. Richardson and Arthur 1988; Patton et al. 1994; Winn et
20 al. 2001), that is consistent with the initiation of basement uplift along the western margin of
21 the Gulf of Suez between 21 and 23 Ma based on fission track analysis (Omar et al. 1989).
22 These very coarse-grained deposits could also be locally related to fault block rotation and
23 exposure of the footwall crests. Sedimentological and structural evidences suggest an overall
24 subdued topography with perhaps only a few hundreds of meters relief that is consistent with
25 previous works (Garfunkel and Bartov 1977; Sellwood and Netherwood 1984).
26
27
28
29
30
31
32
33
34
35
36
37
38
39
40
41
42
43
44
45
46
47
48
49
50

51 *5.3 Rift climax (Miocene, ~Burdigalian, ca. 5Myr duration)*

52 Rotation and uplifting of fault blocks as well as renewing subsidence were recorded all over
53 the basin during the latest Aquitainian-earliest Burdigalian period of time (Post Nukhul Event;
54
55
56
57
58
59
60
61
62
63
64
65

1 Garfunkel and Bartov 1977; Beleity 1984; Chenet et al. 1984). The rift was subdivided into
2 some major basins controlled by active faults highlighting the three main domains of the Suez
3 rift (Figure 5c). Fault linkage still occurred. Tectonic subsidence rates increased (up to 250
4 m/Myr) and the total subsidence rates were as high as 400 m/Myr in the deeper, more rapidly
5 subsiding grabens (Moretti and Colletta 1987; Richardson and Arthur 1988). Subsidence rates
6 in the Gulf of Suez reached their maximum during the Burdigalian and occurred across the
7 entire rift basin (Steckler 1985; Moretti and Colletta 1987; Moretti and Chenet 1987;
8 Richardson and Arthur 1988). Concomitantly, the shoulders of the rift, including the Sinai
9 Massif and Red Sea Hills, underwent rapid uplift (Garfunkel and Bartov 1977; Garfunkel
10 1988).

11 The mid-Clysmic event is interpreted as a major tectonic reactivation in the rift which
12 involved the segmenting and rotation of major pre-existing tilted blocks into smaller units
13 (Garfunkel and Bartov 1977). To the north of the Suez rift, tectonic subsidence ceased
14 completely (Moretti and Colletta 1987; Richardson and Arthur 1988). It corresponds to a
15 major pulse in siliciclastics (at least two times the mean sediment supply during the whole
16 rifting, Figure 6). Moreover, the sediment supply pulse is probably underestimated in our
17 study as we used a duration of 0.9 Myr for R1 and R2 following a simple linear interpolation
18 for the duration of each phases during the Rudeis Fm deposition, while a 0.5 Myr duration
19 would be more likely. It is also concomitant with a major eustatic sea level fall (Gradstein et
20 al. 2012).

21 *5.4 Late syn-rift to rift narrowing (Miocene, ~Langhian-Serravalian, ca. 4Myr duration)*

22 During the Langhian, the rift was subdivided into several main depocenters controlled by
23 active faults that were superimposed onto the previous Rudeis depocenters (Figure 5d). New
24
25
26
27
28
29
30
31
32
33
34
35
36
37
38
39
40
41
42
43
44
45
46
47
48
49
50
51
52
53
54
55
56
57
58
59
60
61
62
63
64
65

1 additional depocenters localized along the rift margin suggest a widely distributed and overall
2 basinal subsidence (Figure 5d).
3

4 The Rudeis to Kareem transition (~ early Langhian) was characterized by a major decrease of
5 the extension rate, especially in the vicinity of Hurghada from 0.48 to 0.18 cm/yr (Steckler et
6 al. 1988). The former reliefs induced during the rift climax were quickly destroyed as
7 evidenced by the drastic drop in sediment supply (Figure 6). Stratigraphic architecture along
8 the eastern margin suggests that some of the main border faults became inactive and fault
9 activity migration toward the basin axis (e.g. Baba area; Figure 3, Figure 4).
10

11 The Kareem to Belayim transition (~ late Langhian) was then characterized by another major
12 decrease of the extension rate from 0.18 to 0.05 cm/yr (Steckler et al. 1988). Subsidence
13 analysis also indicates a sudden drop in subsidence rates at the end of the Kareem Fm
14 deposition (Moretti and Colletta 1987; Richardson and Arthur 1988). During Serravalian
15 times, the rift was subdivided into several main depocenters mainly localized along the
16 present day basin axis (Figure 5e). While tectonic subsidence rate was almost negligible
17 during Serravalian times, accommodation space creation was mainly controlled by sediment
18 loading (Moretti and Colletta 1987) along the basin axis indicating a major rift narrowing
19 (Figure 5e, Figure 6).
20
21
22
23
24
25
26
27
28
29
30
31
32
33
34
35
36
37
38
39
40
41
42

43 *5.5 Tectonic quiescence to latest syn-rift (Miocene, ~Tortonian-Messinian, ca. 7Myr* 44 *duration)* 45

46 The basin was still subdivided into several sub-basins bounded by major faults already well
47 developed during the previous rift narrowing stage (Figure 5f, 5g). Tectonic subsidence was
48 negligible and accommodation space creation was mainly controlled by sediment loading
49 (Moretti and Colletta 1987; Richardson and Arthur 1988). To the north of the Suez rift,
50
51
52
53
54
55
56
57
58
59
60
61
62
63
64
65

1 tectonic uplift could have occurred (Richardson and Arthur 1988). Sedimentary patterns and
2 fauna indicate that the rift was definitively disconnected from the Mediterranean Sea.
3
4
5

6. DISCUSSION

Rift evolution and sediment supply

6
7
8
9
10
11 The large scale evolution of the Suez rift is consistent with other published models for rift
12 evolution with a (1) Rift Initiation, (2) Rift widening, (3) Rift climax, (4) Late syn-rift to rift
13 narrowing and (5) Tectonic quiescence to latest syn-rift (Leeder and Gawthorpe 1987; Prosser
14 1993; Lambiase and Bosworth 1995; Gawthorpe and Leeder 2000). Our study provides some
15 additional constraints in terms of timing and erosion/sedimentation dynamics within the rift
16 evolution (Figure 6). The mass balance analysis indicates that the rift shoulder dynamic
17 includes a growth phase lasting 6-7 Myr recorded by an rapid and progressive increase in
18 sediment supply (Figure 6). Relief then reached its topographic maximum as suggested by the
19 maximum sediment supply (Latest Rudeis Fm, R5). Finally, the rapid and abrupt decrease in
20 sediment supply (ca. 1Myr) during the transition from the Rudeis Fm to Kareem Fm, was
21 followed by a progressive decrease (ca. <3.5Myr duration, Kareem to Belayim Fms) to reach
22 a very low value during the South Gharib Fm deposition. This final evolution can be
23 interpreted as a “relief destruction” phase. This sediment supply dynamic at rift scale is
24 consistent with analog and numerical modeling (growth phase, optimum and destruction
25 phase), clearly indicating that this sediment supply dynamics was tectonically driven (e.g.
26 Lague et al. 2003, Bonnet and Crave 2003, Rohais et al. 2012).
27
28
29
30
31
32
33
34
35
36
37
38
39
40
41
42
43
44
45
46
47
48
49
50

51 This result has a major impact onto the understanding of flank retreat dynamic during post-rift
52 evolution. Indeed, most of the concept and modeling approaches addressing flank retreat issue
53 are based on a starting boundary condition using former rift topography (e.g. van der Beek et
54 al. 1994; Brown et al. 2002; Japsen et al. 2011). In our study, the sediment supply dynamic
55
56
57
58
59
60
61
62
63
64
65

1 indicate that the latest syn-rift phase was characterized by low relief with very localized
2 inputs of siliciclastics (Figure 4, Figure 6). This point could be considered as a major
3
4 challenge in some future works. Typically, in the Suez rift, the present day topography is
5
6 potentially related to the post-rift dynamics.
7
8
9

10 11 *Suez rift and geodynamic setting*

12
13
14 At 14 Ma (Langhian), the Aqaba transform boundary cut through Sinai and the Levant
15
16 continental margin (Figure 1), linking the northern Red Sea with the Bitlis-Zagros
17
18 convergence zone (e.g. Bosworth et al. 2005; Gvirtzman and Steinberg 2012). Extension in
19
20 the Suez was reduced and then stopped (e.g. Moretti and Colletta 1987; Steckler et al. 1988)
21
22 suggesting that the mechanism responsible for the Suez rift opening was no more active.
23
24

25
26 Meanwhile, the opening of the Red Sea continued until became an ocean during the Pliocene.
27
28 Extension in the Suez rift has been previously reduced during the Langhian times in response
29
30 to the collision of Arabia and Eurasia (Dercourt et al., 1986; Le Pichon and Gaulier 1988).
31
32

33
34 The Aqaba transform boundary (Figure 1) could thus be interpreted as an accommodation
35
36 fault between the continuous extensional processes in the southern Red Sea and an abandoned
37
38 extensional segment in the north corresponding to the Suez rift. It suggests that the deep
39
40 source controlling the extension in the Suez rift is not below the rift, but below the Red Sea.
41
42 This is very consistent with a south to north propagation of the Suez rift as documented in our
43
44 reconstruction (Figure 4).
45
46
47
48
49

50 51 *Evaporite in rift basin*

52
53 Evaporite deposition is generally controlled by the combined effect of (1) the hydrologic
54
55 balance, or aridity index and (2) the isolation of the basin characterized by the interaction
56
57 between sill and sea level (e.g. Warren 2010). Regarding the aridity, a global cooling and
58
59
60
61
62
63
64
65

1 drying at about 15.6 Ma (i.e. Langhian) occurred in northeastern Africa (Kennett, 1995). In
2 the late Tortonian – Early Messinian (ca. 8 Ma) relatively more humid conditions occurred in
3
4 an overall arid setting (Griffin, 1999), that is consistent with our reconstructions for the Zeit
5
6 Fm (Messinian). During the Plio/Pleistocene northeastern Africa was still subjected to
7
8 alternating dry and wet periods (Griffin, 1999; 2002). Aridification was thus a criterion
9
10 satisfied for evaporite deposition in the Suez rift starting from the Langhian times.
11
12

13 The main sills were in the north of the Darag basin and across the Zaafarana and Morgan
14
15 accommodation zones (Figure 1). The first evidence for the isolation of the Suez rift occurred
16
17 during the Langhian (Kareem Fm) with a progressive paleo-bathymetry decrease along the
18
19 basin axis (Darag, Central and Southern basins) and the occurrence of a large platform across
20
21 the Central basin (Figure 4h-j). This “Platform Evaporite” *sensu* Warren (2010) has
22
23 progressively been widened to finally reach a “Basinwide Evaporite” *sensu* Warren (2010)
24
25 configuration during the Serravalian times (Belayim Fm). Finally, the main sill controlling the
26
27 disconnection of the Mediterranean Sea from the Red Sea were located in the north of the
28
29 Darag basin during the Tortonian to Messinian times (Figure 4). It indicates that the first sills
30
31 to interact with the sea level changes were related to rift structures: the Zaafarana and Morgan
32
33 accommodation zones. Finally, a sill on the northern edge of the Suez rift was the dominant
34
35 structure controlling the connection between Mediterranean Sea and the Red (Figure 4).
36
37

38 The pre-salt to salt transition in the Suez rift can thus be interpreted as a sedimentary record of
39
40 the combined effect of a climate change (including aridity) and the rift dynamic that lasted for
41
42 ca. 4 Myr. Finally, the occurrence of long lasted and widespread evaporite series where
43
44 controlled by both two major external controlling factors: climate and geodynamic (rift
45
46 abandonment).
47
48
49
50
51
52
53
54
55
56
57

58 *Rift dynamic and sequence stratigraphy*
59
60
61
62
63
64
65

1 A typical rift sequence can be derived from this basin-scale study. The Nukhul Fm with
2 dominantly shallow water deposits can be interpreted as the records of the filled phase, the
3
4 Rudeis Fm with its well-developed turbiditic packages as the underfilled phase, the Kareem
5
6 and Belayim Fms with their prograding patterns and progressive evolution toward shallow
7
8 water deposits as a filled phase and finally the South Gharib and Zeit Fms with the alluvial to
9
10 sabkha deposits as overfilled phase. During filled and overfilled phases, a longitudinal N-S
11
12 depositional gradient prevailed (Figure 4). This tectonically-controlled stratigraphic
13
14 framework can be correlated to a second-order cycle, i.e. 18-20 Myr duration cycle. This
15
16 cycle can be interpreted in a transgressive, highstand and lowstand system tracts sensu
17
18 Catuneanu et al. (2009). At higher resolution, the highstand system tract (Rudeis, Kareem and
19
20 Belayim Fms) can be subdivided into one basal highstand (Lower Rudeis Fm) overlain by a
21
22 falling stage system tract (Upper Rudeis, Kareem and Belayim Fms, Figure 2). This falling
23
24 stage system tract can be subdivided into two third order sequences including two major
25
26 aggrading-prograding packages that can be interpreted as lowstand system tract (Rahmi-
27
28 Markha Mb. and Baba-Sidri-Feiran Mbs.; Figure 2). Duration and timing of these major third
29
30 order sequences are correlated with the main tectonic stage identified for the rift evolution.
31
32
33
34
35
36
37
38
39 The typical rift sequence thus includes: a (1) Rift Initiation, rapid flooding and major
40
41 transgressive surface, (2) Rift widening, transgressive system tract, (3) Rift climax, highstand
42
43 system tract and condensed sections, (4) Late syn-rift to rift narrowing, falling stage system
44
45 tract and (5) Tectonic quiescence to latest syn-rift, lowstand system tract.
46
47

48
49 At higher resolution, i.e. fourth and higher order sequences, the whole cycle is not always
50
51 easily identified. Sequence boundaries are often superimposed by sharp flooding surface
52
53 rapidly overlain by a prograding and shallowing upward packages interpreted as highstand
54
55 system tract (Figure 2). These fourth and higher order sequences could thus be related to stage
56
57 of activity during the fault growth.
58
59
60
61
62
63
64
65

1
2 **7. CONCLUSION**
3

4 Stratigraphic architecture reconstruction have been carried out to propose a basin-scale model
5 evolution for the pre-salt to salt syn-rift fill of the Suez rift. Four main results can be
6
7 highlighted from our study:
8
9

10
11 First, the key periods of time during a rift evolution have been recognized and their durations
12 have been estimated with (1) a rift initiation or onset of the rifting stage (ca. 1-4 Myr
13 duration) with active volcanism and isolated depocenters, (2) a rift widening stage (ca. 3 Myr
14 duration) with a progressive marine flooding and fault propagation, (3) a rift climax (ca. 5
15 Myr duration) characterized by several major anoxic events, maximum fault throw and
16 subsidence rate, increasing and maximum sediment supply from the rift evolution, (4) a late
17 syn-rift to rift narrowing (ca. 4 Myr duration) characterized by a progressive smoothing of the
18 paleogeography with low to no more active tectonic uplift/erosion along the rift shoulders
19 combined with a reducing paleo-bathymetry along the basin axis, (5) and finally a tectonic
20 quiescence phase (ca. 7 Myr duration) characterized by a thick salt series.
21

22
23 Second, the sediment supply dynamics during rifting is characterized by (1) progressive
24 increase up to its (2) maximum, (3) rapid and abrupt decrease (less than 1Myr) and finally (4)
25 very progressive decrease that can be interpreted as a (1) relief growth, (2) optimum and (3, 4)
26 destruction phases related to uplift dynamic.
27

28
29 Third, the pre-salt to salt transition in the Suez rift is interpreted as the sedimentary record of
30 the combined effect of a climate and rift dynamic changes. The Central basin, Zaafarana and
31 Morgan accommodation zones were the first main divides between the Mediterranean Sea and
32 the Red Sea.
33

34
35 Fourth, several order of sequences can be recognized in the syn-rift fill with fourth to higher
36 order sequences related to fault activity, third order sequences related to (sub-)basin dynamics
37
38
39
40
41
42
43
44
45
46
47
48
49
50
51
52
53
54
55
56
57
58
59
60
61
62
63
64
65

1 (Darag, Central and Southern basins) and second order sequences related to the whole rift
2 basin dynamic (Suez rift).
3

4 The proposed geological scenario with quantified sediment supply, accumulation rate,
5 lithologic distribution and subsidence dynamics could be used to test modeling approaches of
6
7 the relationship between deep and surface processes in future works.
8
9

10 11 12 13 **Acknowledgements**

14 This project could not have been accomplished without the very large database acquired by
15
16 IFPEN during the last 30 years in the frame of collaborative partnerships. The authors would
17
18 like to thank the two anonymous reviewers for their valuable suggestions and reviews of the
19
20 initial manuscript.
21
22
23
24
25
26
27
28
29
30
31
32
33
34
35
36
37
38
39
40
41
42
43
44
45
46
47
48
49
50
51
52
53
54
55
56
57
58
59
60
61
62
63
64
65

1 Abdelghany O (2002) Lower Miocene stratigraphy of the Gebel Shabrawet area, north
2 Eastern desert Egypt. *Journal of African Earth Sciences* 34 (2002) 203–212

3 Abd El-Naby AIM, Ghanem H, Boukhary M, Abd El-Aal M, Lüning S, Kuss J (2010)
4 Sequence-stratigraphic interpretation of structurally controlled deposition: Middle Miocene
5 Kareem Formation, southwestern Gulf of Suez, Egypt: *GeoArabia.*, 15(3): 129-150
6

7
8 Abd El Shafy A (1990) Miocene-Pliocene boundary in the Gulf of Suez region, Egypt. 10th
9 EGPC Exploration Seminar, Cairo, Egypt, 1:213-233
10

11
12 Allen G, Ayyad A, Desforges G, Haddadi M, Pizon J (1984) Subsurface sedimentological
13 study of the Rudeis Formation in Kareem, Ayun, Yusr and Shukheir fields, in *Proceedings of*
14 *the 6th Exploration Conference: Cairo, Egyptian General Petroleum Corporation*, p. 164–176
15

16
17 Artushkov E and Baer M (1984) Mechanism of continental crust subsidence in the Alpine
18 Belt. *Tectonophysics*, V 108, 193-228
19

20
21 Barrois A (2011) Couplage d'un modèle structural 3D restauré (Kiné3D-3) avec un modèle de
22 remplissage stratigraphique (Dionisos) en contexte extensif, cas du rift de Suez (Égypte).
23 I.F.P. report 62044
24

25
26 Barrois A, Rohais S, Granjeon D, Rudkiewicz JL, Cacas MC (2010) Coupling 3D Structural
27 Restoration with Stratigraphic Modelling in Rifted Margins, Suez Rift, Egypt. International
28 conference "Modelling sedimentary basins and their petroleum systems", June 3-4th 2010,
29 Geol. Soc. London
30

31
32 Beleity AM (1984) The composite standard and definition of paleogeography and
33 paleotectonics in the Gulf of Suez. In *Egyptian General Petroleum Corporation. 6th EGPC*
34 *Exploration Conference, Cairo, Egypt*, 181–198
35

36
37 Bonnet S and Crave A (2003) Landscape response to climate change: insights from
38 experimental modeling and implications for tectonic vs. climatic uplift of topography.
39 *Geology* 31: 123–126
40

41
42 Bosence DWJ, Cross NE, Hardy S (1998) Architecture and depositional sequences of Tertiary
43 fault-block carbonate platforms; an analysis from outcrop and computer modelling. *Mar Pet*
44 *Geol*;15:203– 21
45

46
47 Bosworth W (1995) A high-strain rift model for the southern Gulf of Suez. Egypt. In J.J.
48 Lambiase (Ed.), *Hydrocarbon habitat in rift basins*. Geological Society, London, special
49 publication no. 80, p. 75-112
50

51
52 Bosworth W, Crerello P, Winn Jr RD, Steinmetz J (1998) Structure, sedimentation, and basin
53 dynamics during rifting of the Gulf of Suez. In: Purser BH, Bosence DWJ (eds)
54 *Sedimentation and tectonics of rift basins: Red Sea–Gulf of Aden*. pp. 78–96
55

56
57 Bosworth W and McClay K (2001) Structural and stratigraphic evolution of the Gulf of Suez
58 rift, Egypt: a synthesis. In: Ziegler PA, Cavazza W, Roberston AHF, Crasquin-Soleau S (eds)
59 *Peri-Tethys Memoir 6: Peri-Tethyan rift/wrench basins and passive margins*. p. 567–606
60
61
62
63
64
65

1 Bosworth W, Huchon P, McClay K (2005) The Red Sea and Gulf of Aden Basins. *J. Afr.*
2 *Earth Sci.* 43, 334–378

3 Brown RW, Summerfield MA, Gleadow AJW (2002) Denudational history along a transect
4 across the Drakensberg Escarpment of southern Africa derived from apatite fission track
5 thermochronology. *J. Geophys. Res.-Solid* 107, 74–77

6
7
8 Bunter MAG (1980) Gulf of Suez Stratigraphic Summary, CONOCO Internal Report

9
10 Burchette TP (1987) Tectonic control on carbonate platform facies distribution and sequence
11 stratigraphy: Miocene, Gulf of Suez. *Sedimentary Geology*, v. 59, p. 179-204

12
13 Burov EB and Poliakov ANB (2001) Erosion and rheology controls on syn- and post-rift
14 evolution: Verifying old and new ideas using a fully coupled numerical model, *J. Geophys.*
15 *Res.*, 106, 16,461–16,481

16
17
18 Catuneanu O, Abreu V, Bhattacharya JP, Blum MD, Dalrymple RW, Eriksson PG, Fielding
19 CR, Fisher WL, Galloway WE, Gibling MR, Giles KA, Holbrook JM, Jordan R, Kendall
20 CGStC, Macurda B, Martinsen OJ, Miall AD, Neal JE, Nummedal D, Pomar L, Posamentier
21 HW, Pratt BR, Sarg JF, Shanley KW, Steel RJ, Strasser A, Tucker ME, Winker C (2009)
22 Towards the Standardization of Sequence Stratigraphy. *Papers in the Earth and Atmospheric*
23 *Sciences*. Paper 238

24
25
26 Chaboureau AC, Guillocheau F, Robin C, Rohais S, Moulin M, Aslanian D (2013)
27 Paleogeographic evolution of the central segment of the South Atlantic during Early
28 Cretaceous times: paleotopographic and geodynamic implications. *Tectonophysics* 604, 191–
29 223

30
31
32 Chenet PY (1984) Tectonics of the Suez rift; structural analysis of the Nukhul area. I.F.P.
33 report n°32118

34
35
36 Chenet PY, Letouzey J, Zaghoul E (1984) Some observations on the rift tectonics in the
37 eastern part of the Suez rift. *Proceedings of the 7th Egyptian General Petroleum Corporation*
38 *Exploration Seminar, Cairo, Egypt 1984:18-36*

39
40
41 Chowdhary LR, Shaheen S, Naggar AA (1986) Structure and structural evolution of Ras
42 Budran, Gulf of Suez, Egypt. 8th E.G.P.C. Explor. Conf.. Cairo. Preprint.

43
44
45 Cloetingh S, Tibaldi A and Burov E (2012) Coupled Deep Earth and surface processes and
46 their impact on geohazards. *Global and Planetary Change* 90–91 (2012) 1–19.
47 doi:10.1016/j.gloplacha.2012.01.010

48
49
50 Colletta B, LeQuellec P, Letouzey J, Moretti I (1988). Longitudinal evolution of the Suez rift
51 structure (Egypt). *Tectonophysics* 153, 221-233

52
53
54 Cowie PA, Gupta S, Dawers, NH (2000) Implications of fault array evolution for syn-rift
55 depocentre development: insights from a numerical fault growth model. *Basin Research*, 12:
56 241–261. doi:10.1111/j.1365-2117.2000.00126.x

57
58
59
60
61
62
63
64
65

1 Dercourt J, Zonenshain LP, Ricou LE, Kazmin VG, Le Pichon X, Knipper A, Grandjacquet
2 C, Shortshikov IM, Geyssant J, Lepvrier C, Perchersky DH, Boulin J, Sibuet J-C, Savostin
3 LA, Sorokhtin O, Westphal M, Bazhenov ML, Lauer JP, Biju-Duval B (1986) Geological
4 evolution of the Tethys belt from the Atlantic to the Pamirs since the Lias. *Tectonophysics*
5 123, 241–315
6

7 El Beialy SY and Ali AS (2002) Dinoflagellates from the Miocene Rudeis and Kareem
8 formations borehole GS-78-1, Gulf of Suez, Egypt. *Journal of African Earth Sciences*, 35,
9 235-245.
10

11 El Beialy SY, Mahmoud MS, Ali AS (2005) Insights on the age, climate and depositional
12 environments of the Rudeis and Kareem formations, GS-78-1 well, Gulf of Suez, Egypt: A
13 Palynological Approach. *Revista Española de Micropaleontología.*, 37(2): 273-289
14
15

16 El Shinnawi MA (1975) Planktonic foraminifera from the Miocene Globigerina Marl of
17 Hurgada Well-134, Eastern Desert, Egypt. In: Mineras ENAdI (ed) 5th African Colloquium
18 on Micropalaeontology, Addis Ababa, pp 199–224
19
20

21 Egyptian General Petroleum Corporation, EGPC (1964) Oligocene and Miocene rock-
22 stratigraphy of the Gulf of Suez region, report of the Stratigraphic Committee: Egyptian
23 General Petroleum Corporation, 142 pp
24
25

26 Evans AL (1988) Neogene tectonic and stratigraphic events in the Gulf of Suez rift area,
27 Egypt. *Tectonophysics* 153:235-247
28
29

30 Evans AL (1990) Miocene sandstone provenance relations in the Gulf of Suez: Insights into
31 syn-rift unroofing and uplift history, *AAPG Bull.*, 74, 1386-1400
32
33

34 Fawzy H and Abdel Aal A (1984) Regional study of Miocene evaporates and Pliocene–recent
35 sediments in the Gulf of Suez. In Egyptian General Petroleum Corporation. 7th EGPC
36 Exploration Seminar, Cairo, Egypt, 49–74
37
38

39 Fleitout L and Yuen D (1984) Steady State secondary convection beneath lithospheric plates
40 with temperature and pressure dependent viscosity. *JGR*, 89, 9227-9244
41
42

43 Garfunkel Z and Bartov Y (1977) The tectonics of the Suez rift. *Geol Surv Isr Bull* 71:45
44

45 Garfunkel Z (1988) Relation between continental rifting and uplifting: evidence from the
46 Suez rift and northern Red Sea. *Tectonophysics*, v. 150, pp. 33-49
47
48

49 Gargani J, Moretti I, Letouzey J (2008) Evaporite accumulation during the Messinian Salinity
50 Crisis: The Suez Rift case, *Geophys. Res. Lett.*, 35, L02401, doi:10.1029/2007GL032494
51
52

53 Gawad WA, Gaafar I, Sabour AA (1986) Miocene stratigraphic nomenclature in the G.O.S.
54 region. 8th E.G.P.C. Explor. Conf., Cairo. Preprint.
55

56 Gawthorpe RL, Hurst JM, Sladen CP (1990) Evolution of Miocene footwall derived coarse-
57 grained deltas. Gulf of Suez, Egypt: implications for exploration. *Bulletin of the American*
58 *Association of Petroleum Geologists*, v. 74, p. 1077-1086
59
60
61
62
63
64
65

1 Gawthorpe RL, Sharp I, Underhill JR, Gupta S (1997) Linked sequence stratigraphic and
2 structural evolution of propagating normal faults. *Geology*, 25, 795–798

3 Gawthorpe RL and Leeder MR (2000) Tectono-sedimentary evolution of active extensional
4 basins. *Basin Research*, v. 12, p. 195-218

5
6
7 Gawthorpe RL, Jackson CAL, Young MJ, Sharp IR, Moustafa AR (2003) Fault growth,
8 interaction, linkage and death: evolution of the Hammam Faraun fault block, Suez rift, Egypt.
9 *Journal of Structural Geology*, 25, 883–895.

10
11
12 Ghorab MA (1964) Oligocene and Miocene rock stratigraphy of the Gulf of Suez region,
13 unpublished report consultatus stratigraphic committee of the EGPC., Cairo, E.R., 275pp

14
15
16 Gradstein FM, Ogg JG, Schmitz MD, Ogg GM (2012) *The Geologic Time Scale*. Elsevier
17 [doi:10.1016/B978-0-444-59425-9.10003-4](https://doi.org/10.1016/B978-0-444-59425-9.10003-4)

18
19 Griffin DL (1999) The late Miocene climate of north-eastern Africa: unravelling the signals in
20 the sedimentary succession: *Journal of the Geological Society*, v. 156, p. 817–826

21
22
23 Griffin DL (2002) Aridity and humidity: two aspects of the late Miocene climate of North
24 Africa and the Mediterranean. *Palaeogeography, Palaeoclimatology, Palaeoecology* 182, 65-
25 91

26
27
28 Guillocheau F, Rouby D, Robin C, Helm C, Rolland N, Le Carlier de Veslud C, Braun J
29 (2012) Quantification and causes of the terrigenous sediment budget at the scale of a
30 continental margin: a new method applied to the Namibia–South Africa margin. *Basin*
31 *Research*, 24: 3–30. doi: 10.1111/j.1365-2117.2011.00511.x

32
33
34 Gupta S, Cowie PA, Dawers NH, Underhill JR (1998) A mechanism to explain rift basin
35 subsidence and stratigraphic patterns through fault array evolution. *Geology*, 26, 595–598

36
37
38 Gupta S, Underhill JR, Sharp IR, Gawthorpe RL (1999) Role of fault interactions in
39 controlling synrift sediment dispersal patterns: Miocene Abu Alaqa Group, Suez Rift, Sinai,
40 Egypt. *Basin Research*, v. 11. p. 167-189

41
42
43 Gvirtzman Z and Steinberg J (2012) Inland jump of the Arabian northwest plate boundary
44 from the Levant continental margin to the Dead Sea Transform. *Tectonics* 31, TC4003

45
46 Hagra M and Slocki S (1982) Sand distribution of Miocene clastics in the Gulf of Suez. In:
47 HANTAR, G. (ed.) Egyptian General Petroleum Company 6th Exploration Seminar Preprint

48
49
50 Halim M, Said M, El Azhary T (1996) 13th Petroleum Conference, Vol. I: Exploration, 401-
51 420, Oct. 1996, Cairo.

52
53
54 Hagra M (1986) Some geological observations in the Gulf of Suez. 8th Petrol. Explor.
55 Seminar, E.G.P.C., Cairo, 1-12.

56
57
58 Haines SS, Klempner SL, Brown L, Jingru G, Mechie J, Meissner R, Ross A, Wenjin Z
59 (2003) INDEPTH III seismic data: From surface observations to deep crustal processes in
60 Tibet, *Tectonics*, 22, 1001, doi:10.1029/2001TC001305, 1

1 Helmy M and Zakaria A (1986) El Morgan area geologic framework. Proc. 8th Petrol. Explor.
2 Seminar, E.G.P.C., Cairo
3

4 Hughes GW, Abdine S, Girgis MH (1992) Miocene biofacies development and geological
5 history of the Gulf of Suez, Egypt. *Mar Pet Geol* 9:27
6
7

8 Jackson CAL, Gawthorpe RL, Sharp IR (2002) Growth and linkage of the East Tanka fault
9 zone, Suez rift: structural style and syn-rift stratigraphic response. *Journal of Geological*
10 *Society, London*, 159, 175–187
11

12 Jackson CAL, Gawthorpe RL, Carr ID, Sharp IR (2005) Normal faulting as a control on the
13 stratigraphic development of shallow marine syn-rift sequences: the Nukhul and Lower
14 Rudeis Formations, Hammam Faraun fault block, Suez Rift, Egypt. *Sedimentology*, v. 52. p.
15 313-338
16
17

18 Japsen P, Chambers JA, Green PF, Bonow JM (2011) Elevated, passive continental margins:
19 Not rift shoulders, but expressions of episodic, post-rift burial and exhumation: *Global and*
20 *Planetary Change*, 2011
21
22

23 Kappelman J, Simons EL, Swisher III CC (1992) New age determinations for the Eocene–
24 Oligocene boundary sediments in the Fayum Depression, northern Egypt. *Journal of Geology*
25 100, 647–668
26
27

28 Khalil SM and McClay KR (2002) Extensional fault-related folding, northwestern Red Sea,
29 Egypt. *Journal of Structural Geology*, 24, 743–762
30
31

32 Khaled D, Sehim A, Darwish M (2002) Rift architecture and growth sedimentation across a
33 main accommodation zone, Northern Gulf of Suez – Egypt. *Inter. Petroleum Conference and*
34 *Exhibition, AAPG 2002, Cairo, Egypt*
35
36

37 Kohn BP and Eyal M (1981) History of uplift of the crystalline basement of Sinai and its
38 relation to opening of the Red Sea as revealed by fission track dating of apatites, *Earth Planet.*
39 *Sci. Lett.* 52, 129-141
40
41

42 Krebs WN, Wescott D, Nummedahl I, Gaafar G, Azazi G, Karamat S (1997) Graphic
43 correlation and sequence stratigraphy of Neogene rocks in the Gulf of Suez. In *Fauna, flora*
44 *and sequence stratigraphy. Association Paleontologie Francaise de Stratigraphie*, v. 168, no. 1,
45 p. 64-71
46
47

48 Lague D, Crave A, Davy P (2003) Laboratory experiments simulating the geomorphic
49 response to tectonic uplift. *J. Geophys. Res.* 108, B1
50
51

52 Lambiase JJ and Bosworth W (1995) Structural controls on sedimentation in continental rifts.
53 In: Lambiase, J.J. (Ed.), *Hydrocarbon Habitat in Rift Basins*, Geological Society, London,
54 *Special Publication 80*, 117–144
55
56

57 Leeder MR and Gawthorpe RL (1987) Sedimentary models for extensional tilt-block/half-
58 graben basins. In M.P. Coward, J.F. Dewey and P.L. Hancock (Eds.), *Continental extensional*
59 *tectonics. Geological Society of London Special Publication No. 28*, p. 139-152
60
61
62
63
64
65

1 Le Pichon X and Gaulier J-M (1988) The rotation of Arabia and the Levant fault system.
2 Tectonophysics 153, 271–294
3

4 Le Quellec P and Colletta B (1985) Synthèse structurale sur le rift du Golfe de Suez. Report
5 C.F.P./I.F.P., I.F.P. report 33724
6

7
8 Leroy S, Razin P, Autin J, Bache F, d'Acremont E, Watremez L, Robinet J, Baurion C,
9 Denèle Y, Bellahsen N, Lucazeau F, Rolandone F, Rouzo S, Serra Kiel J, Robin C et al.
10 (2012) From rifting to oceanic spreading in the Gulf of Aden: a synthesis. Arab J.
11 Geosciences. DOI 10.1007/s12517-011-0475-4, vol 5, 859-901
12

13
14 Lotfy HI, Van der Voo R, Hall CM, Kamel OA, Abdel Aal AY (1995). Palaeomagnetism of
15 Early Miocene basaltic eruptions in the areas east and west of Cairo. Journal of African Earth
16 Sciences 21, 407–419
17

18
19 Lyberis N (1988) Tectonic evolution of the Gulf of Suez and the Gulf of Aqaba.
20 Tectonophysics, 153, 209–220
21

22
23 McKenzie D (1978) Some remarks on the development of sedimentary basins. Earth and
24 Planet Sci Lett 40:25–32
25

26
27 Macgregor D (2015) History of the development of the East African Rift System: A series of
28 interpreted maps through time. Journal of African Earth Sciences 101 (2015) 232–252
29

30
31 Mann P, Gahagan L, Gordon MB (2003) Tectonic setting of the world's giant oil and gas
32 fields, in M. T. Halbouty, ed., Giant oil and gas fields of the decade 1990–1999, AAPG
33 Memoir 78, p. 15–105
34

35
36 Martin J, Toothill S, Moussavou R (2009) Hunting the pre-salt. Frontier Exploration. Geo
37 Expro Dec. 2006. 39-41
38

39
40 McClay KR, Nichols GJ, Khalil S, Darwish M, Bosworth W (1998) Extensional tectonics and
41 sedimentation, eastern Gulf of Suez. Egypt. In B.H. Purser and D.W.J. Bosence (Eds.),
42 Sedimentation and tectonics of rift basins, Red Sea-Gulf of Aden: Chapman and Hall,
43 London, p. 223-238
44

45
46 Montenat C, Ott d'Estevou P, Purser BH (1986) Tectonic and sedimentary evolution of the
47 Gulf of Suez and the Northwestern Red Sea: a review. Dot. Trav. I.G.A.L., Paris, 10: 7-18
48

49
50 Montenat C, Ott d'Estevou P, Purser B, Buroillet PF, Jarrige J-J, Orszag-Sperber F, Philobos
51 E. Plaziat JC, Prat P, Richert J-P, Roussel N, Thiriet J-P (1988) Tectonic and sedimentary
52 evolution of the Gulf of Suez and the Northwestern Red Sea. Tectonophysics, v. 153, p. 161-
53 177
54

55
56 Moretti I and Froidevaux C (1986) Thermomechanical models of active rifting. Tectonics, 3,
57 501-511
58

59
60 Moretti I (1987) Modélisation de l'extension intracontinentale : exemple du golfe de suez.
61 I.F.P. report 34961
62
63
64
65

1 Moretti I and Chenet PY (1987) The evolution of the Suez rift: a combination of stretching
2 and secondary convection: *Tectonophysics*, v. 133, p. 229-234
3

4 Moretti I and Colletta B (1987) Spatial and temporal evolution of the Suez Rift subsidence. *J.*
5 *Geodyn.* 7, 151–168
6

7
8 Moretti I and Pinet B (1987) Discrepancy between lower and upper crustal thinning. In
9 *Sedimentary basins and basin-forming mechanisms*. Canadian Society of PG, Memoir 12,
10 233-239
11

12
13 Moussa HE (1987) Geologic studies and genetic correlation of basaltic rocks in west central
14 Sinai. PhD thesis, Ain Shams University, Cairo, Egypt
15

16
17 Moustafa AG (1976) Block faulting in the Gulf of Suez. *Proceedings of the 5th Petroleum*
18 *Exploration and Production Seminar, Egypt*, v. 1, 19p.
19

20
21 Moustafa AR (1993) Structural characteristics and tectonic evolution of the east-margin
22 blocks of the Suez rift. *Tectonophysics* 223, 381-399
23

24
25 Moustafa AR (1996) Internal structure and deformation of an accommodation zone in the
26 northern part of the Suez rift. *Journal of Structural Geology*, 18, 93–107
27

28
29 Omar GI, Steckler MS, Buck WR, Kohn BP (1989) Fission-track analysis of basement
30 apatites at the western margin of the Gulf of Suez rift, Egypt: evidence for synchronicity of
31 uplift and subsidence. *Earth Planet. Sci. Lett.* 94, 316–328
32

33
34 Omran MA and El Sharawy MS (2014) Tectonic evolution of the Southern Gulf of Suez,
35 Egypt: a comparison between depocenter and near peripheral basins. *Arab J Geosci* (2014)
36 7:87–107. DOI 10.1007/s12517-012-0732-1
37

38
39 O'Reilly C, Chisari D, Clarke J, Musa S, Halliday J, Deighton I, Tobochoa E, Chandler P
40 (2015) Comparing the Brazilian and Angolan Conjugate Margin. *GeoExpro* Oct. 2015. 61-62
41

42
43 Orszag-Sperber F, Harwood G, Kendall A, Purser BH (1998) A review of the evaporites of
44 the Red Sea-Gulf of Suez rift. In, B.H. Purser and D.W.J. Bosence (Eds.), *Sedimentation and*
45 *Tectonics in Rift Basins: Red Sea-Gulf of Aden*. Chapman and Hall, London, p. 409-426
46

47
48 Patton TL, Moustafa AR, Nelson RA, Abdine SA (1994) Tectonic evolution and structural
49 setting of the Suez Rift. In S.M. London (Ed.), *Interior rift basins*. American Association of
50 *Petroleum Geologists Memoir No. 59*, p. 7-55
51

52
53 Peijs JAMM, Bevan TG, Piombino JT (2012) The Gulf of Suez rift basin. In D.G. Roberts
54 (Ed.), *Regional Geology and Tectonics: Phanerozoic Rift Systems and Sedimentary Basins*. p.
55 164-194. [doi:10.1016/B978-0-444-56356-9.00007-9](https://doi.org/10.1016/B978-0-444-56356-9.00007-9)
56

57
58 Piron E (2000) Géométrie des failles normales dans le golfe de Suez (Sinai, Égypte). *Aspect*
59 *2D en coupe verticale*. I.F.P. report 54139
60
61
62
63
64
65

1 Plaziat JC, Montenat C, Barrier P, Janin MC, Orszag-Sperber F, Philobos E (1998)
2 Stratigraphy of the Egyptian syn-rift deposits: correlations between axial and peripheral
3 sequences of the north-western Red Sea and Gulf of Suez and their relations with tectonics
4 and eustacy. In, B.H. Purser and D.W.J. Bosence (Eds.), *Sedimentation and Tectonics in Rift
5 Basins: Red Sea-Gulf of Aden*. Chapman and Hall, London, p. 211-222
6

7 Poag CW and Sevon WD (1989) A record of Appalachian denudation in Post-Rift Mesozoic
8 and Cenozoic sedimentary deposits of the U.S. Middle Atlantic Continental margin.
9 *Geomorphology*, 2, 119-157
10

11 Prosser S (1993) Rift-related linked depositional systems and their seismic expression. In:
12 Williams, G.D. & Dobb, A. (eds) *Tectonics and Seismic Sequence Stratigraphy*. Geological
13 Society, London, Special Publications, 71, 35–66
14
15

16 Purser BH and Hötzl H (1988) The sedimentary evolution of the Red Sea rift: a comparison of
17 the northwest (Egyptian) and northeast (Saudi Arabian) margins. *Tectonophysics* 153:193–
18 208
19
20

21 Richardson M and Arthur MA (1988) The Gulf of Suez-northern Red Sea Neogene rift: a
22 quantitative basin analysis. *Marine Pet. Geol.* 5, 247–270
23
24

25 Rohais S, Eschard R, Ford M, Guillocheau F, Moretti I (2007a) Stratigraphic architecture of
26 the Plio-Pleistocene Infill of the Corinth rift: implications for its structural evolution.
27 *Tectonophysics* 440, 5-28
28
29

30 Rohais S, Colletta B, Moretti I (2007b) The Gulf of Suez: Regional setting, petroleum system
31 and tectonic-sedimentation relationship. Field guide, Nov. 2007. Unpublished IFPEN report
32
33

34 Rohais S, Bonnet S, Eschard R (2012) Sedimentary record of tectonic and climatic erosional
35 perturbations in an experimental coupled catchment-fan system. *Basin Research*, 24: 198–
36 212. doi: 10.1111/j.1365-2117.2011.00520.x
37
38

39 Rohais S, Barrois A, Colletta B, Moretti I (2013) Architecture stratigraphique et évolution
40 paléogéographique du Golfe de Suez : Apports de l'enregistrement sédimentaire sur la
41 dynamique d'un rift. 14ème congrès français de sédimentologie. 5-7 novembre 2013, Paris :
42 Centre des congrès de la Vilette
43
44

45 Rohais S, Barrois A, Colletta B, Moretti I (2015) Presalt to Salt Paleogeography and
46 Stratigraphic Architecture in a Rift Basin: Insights From a Basin-Scale Study of the Gulf of
47 Suez (Egypt). AAPG Datapages/Search and Discovery Article #90217 © 2015 International
48 Conference & Exhibition, Melbourne, Australia, September 13-16, 2015
49
50

51 Rouby D, Bonnet S, Guillocheau F, Gallagher K, Robin C, Biancotto F, Dauteuil O, Braun J
52 (2009) Sediment supply to the Orange sedimentary system over the last 150 My: an evaluation
53 from sedimentation/denudation balance. *Mar. Petrol. Geol.*, 26, 782-794
54
55

56 Rouchy JM, Nod D, Wali AMA, Aref MAM (1995) Evaporitic and biosiliceous cyclic
57 sedimentation in the Miocene of the Gulf of Suez-depositional and diagenetic aspects.
58 *Sediment Geol* 94:277–297
59
60
61
62
63
64
65

1 Salah MG and Alsharhan AS (1997) The Miocene Kareem Formation in the southern Gulf of
2 Suez, Egypt: a review on stratigraphy and petroleum geology. *Journal of Petroleum Geology*,
3 v. 20, no. 3, p. 327-346

4 Sarhan MA, Richard Ell, Collier RELI, Basal A, Abdel Aal MH (2014) Late Miocene normal
5 faulting beneath the northern Nile. Delta: NNW propagation of the Gulf of Suez Rift. *Arab J*
6 *Geosci* (2014) 7:4563–4571. DOI 10.1007/s12517-013-1089-9

7 Saoudi A and Kalil B (1984) Distribution and hydrocarbon potential of Nukhul sediments in
8 the Gulf of Suez. In Egyptian General Petroleum Corporation. 7th EGPC Exploration
9 Seminar, Cairo, Egypt, 75-96

10 Schütz KI (1994) Structure and stratigraphy of the Gulf of Suez, Egypt. In S. M. Landon
11 (Ed.), Interior rift basins. American Association of Petroleum Geologists Memoir No. 59, p.
12 57-96

13 Scott RW and Govean FM (1985) Early depositional history of a rift basin: Miocene in
14 western Sinai. *Palaeogeogr. Palaeoclimatol. Palaeoecol.* 62, 143-158

15 Sellwood BW and Netherwood RE (1984) Facies evolution in the Gulf of Suez area:
16 sedimentation history as an indicator of rift initiation and development *Modern Geol.* 9, 43-69

17 Sleep N, Nunn J, Chou L (1980) Platform basins, annual *Reviews of Earth and Planetary*
18 *Science*, V 8, 17-34

19 Smale JLR, Thunell C, Schamel S (1988) Sedimentologic evidence for early Miocene fault
20 reactivation in the Gulf of Suez: *Geology*, v. 16, p. 113–116

21 Steckler MS (1985) Uplift and extension at the Gulf of Suez: indications of induced mantle
22 convection. *Nature* 317, 135–139

23 Steckler MS, Bertholot F, Lyberis N, Le Pichon X (1988) Subsidence in the Gulf of Suez:
24 implications for rifting and plate kinematics. *Tectonophysics* 153, 249–270

25 Thiriet JP (1987) Evolution tectonique et sédimentaire de la marge occidentale de la Mer
26 Rouge au Néogène de Port Safaga (Egypte), PhD, 1333pp., Univ. Claude-Bernard, Lyon,
27 France

28 van der Beek P, Cloetingh S, Andriessen P (1994) Mechanisms of extensional basin formation
29 and vertical motions at rift flanks: constraints from tectonic modeling and fission-track
30 thermochronology. *Earth Planet. Sci. Lett.* 121, 417–433

31 Warren JK (2010) Evaporites through time: Tectonic, climatic and eustatic controls in marine
32 and nonmarine deposits: *Earth-Science Reviews*, v. 98/3-4, p. 217-268

33 Wernicke B (1985) Uniform-sense normal simple shear of the continental lithosphere.
34 *Canadian Journal of Earth Sciences*, 1985, 22:108-125, 10.1139/e85-009

35 Wescott WA, Krebs WN, Sikora PJ, Boucher PJ, Stein SA (1998) Modern applications of
36 biostratigraphy in exploration and production. *The Leading Edge*. Oct. 1998, 1204-1210

37
38
39
40
41
42
43
44
45
46
47
48
49
50
51
52
53
54
55
56
57
58
59
60
61
62
63
64
65

1 Winn RD, Crevello PD, Bosworth W (2001) Lower Miocene Nukhul Formation, Gebel el
2 Zeit, Egypt: Model for structural control on early synrift strata and reservoirs, Gulf of Suez.
3 Bulletin of the American Association of Petroleum Geologists, v. 85, no. 10, p. 1871-1890
4

5
6 Young MJ, Gawthorpe RL, Sharp IR (2000) Sedimentology and sequence stratigraphy of a
7 transfer zone coarse-grained delta, Miocene Suez Rift, Egypt. Sedimentology, v. 47, p. 1081-
8 1104
9

10
11 Young MJ, Gawthorpe RL, Sharp IR (2003) Normal fault growth and early syn-rift
12 sedimentology and sequence stratigraphy: Thal Fault, Suez Rift, Egypt. Basin Research, 15,
13 479–502.
14

15
16 Zierenberg RA and Shanks III WC (1986) Isotopic constraints on the origin of the Atlantis II,
17 Suakin and Valdivia brines, Red Sea, Geochem. Cosmochim. Acta 50, 2205-2214
18
19
20
21
22
23
24
25
26
27
28
29
30
31
32
33
34
35
36
37
38
39
40
41
42
43
44
45
46
47
48
49
50
51
52
53
54
55
56
57
58
59
60
61
62
63
64
65

FIGURE CAPTION

Figure 1

A. Structural map of the Suez rift (modified from Colletta et al. 1988; Patton et al. 1994; Bosworth and McClay 2001; Peijs et al. 2012). Hatched areas indicate major accommodation zones. Red lines correspond to the two cross sections presented in Figure 3. B. Geodynamic setting of the Gulf of Suez (modified from Bosworth et al. 2005). Major elements of the Aqaba–Levant intra-continental transform boundary, the Bitlis-Zagros convergence zone and the Red Sea – Gulf of Aden are highlighted. The red rectangle shows the Gulf of Suez that corresponds to the NW termination of the Red Sea. C. Simplified stratigraphic column of the Suez rift (modified from EGPC 1964; Richardson and Arthur 1988; Patton et al. 1994; Bosworth and McClay 2001; Abd El-Naby et al. 2010).

Figure 2

Synthetic stratigraphic setting for the syn-rift succession of the Suez rift. Lithologies are derived from different wells to illustrate the typical sedimentary character of each formation. Silty rich for restricted deposits in green versus mud rich for offshore deposits in light blue. The association zones, main environment of deposition (EOD) and dominant paleoenvironmental conditions are modified from Hughes et al. (1992). Sequences are modified from Wescott et al. (1998) and Krebs et al. (1997). Colour code for system tracts: blue= transgressive, red= highstand and falling stage, orange= lowstand.

Figure 3

(A) and (B) N-S cross sections flattened on the top Zeit marker (locally base Pliocene when top Zeit Fm is not preserved) showing the distribution of the main depositional units (A) and the dominant lithologies (B) within each sub-basins and across the two accommodation zones. (C) and (D) E-W cross section flattened on the top Zeit marker (locally base Pliocene when top Zeit Fm is not preserved) showing the distribution of the main depositional units (C) and the dominant lithologies (D) within the Central Basin. Sections cross-cut at well 13.

Figure 4

Maps with dominant lithologies for the Nukhul Fm (a-c, ca. Aquitanian), Rudeis Fm (d-g, ca. Burdigalian), Kareem Fm (h-k, ca. Langhian), Belayim Fm (l-o, ca. Serravallian), South Gharib Fm (p-q, ca. Tortonian) and Zeit Fm (r-s, ca. Messinian). Time intervals are approximated using association zones from Hughes et al. (1992). Shales are subdivided into silty rich for restricted deposits in green versus mud rich for offshore deposits in light blue. Paleobathymetries are estimated using the results of Hughes et al. (1992). Only the deepest parts are highlighted to keep the maps readable. See Figure 1 for further information about the keys.

Figure 5

Main depocenters and distribution of the syn-rift deposits for the main stratigraphic units of the Suez rift. a. Oligocene – Chattian. b. Nukhul Fm, cut-off to highlight depocenters at 300 m. c. Rudeis Fm, cut-off to highlight depocenters at 1000 m. d. Kareem Fm, cut-off to highlight depocenters at 400 m. e. Belayim Fm, cut-off to highlight depocenters at 200 m. f. South Gharib Fm, cut-off to highlight depocenters at 900 m. g. Zeit Fm, cut-off to highlight depocenters at 600 m. See Figure 1 for further information about the keys.

Figure 6

1 Synthesis for the pre-salt and salt deposits of the Suez rift of evaporite and carbonate
2 accumulation rate (km^3/Myr), mean sediment supply (km^3/Myr) and cumulative tectonic
3 subsidence curves (modified from the wells analysed by Moretti and Colletta 1987;
4 Richardson and Arthur 1988). The grey area includes all the wells analysed for estimating the
5 cumulative tectonic subsidence. The chronostratigraphy, microfossil biozones and sea-level
6 curve are derived from Gradstein et al. (2012). Relative proportions of lithology for each map
7 have been combined with thickness map to estimate the accumulation rate and sediment
8 supply. See text for further information.
9

10
11
12
13
14
15
16 TABLE CAPTION

17
18 Table 1
19 Results of the mass balance characterization of the pre-salt to salt syn-rift deposits of the Suez
20 rift. The preferred scenario is highlighted in grey. See text for further explanation.
21
22
23
24
25
26
27
28
29
30
31
32
33
34
35
36
37
38
39
40
41
42
43
44
45
46
47
48
49
50
51
52
53
54
55
56
57
58
59
60
61
62
63
64
65

Figure 2

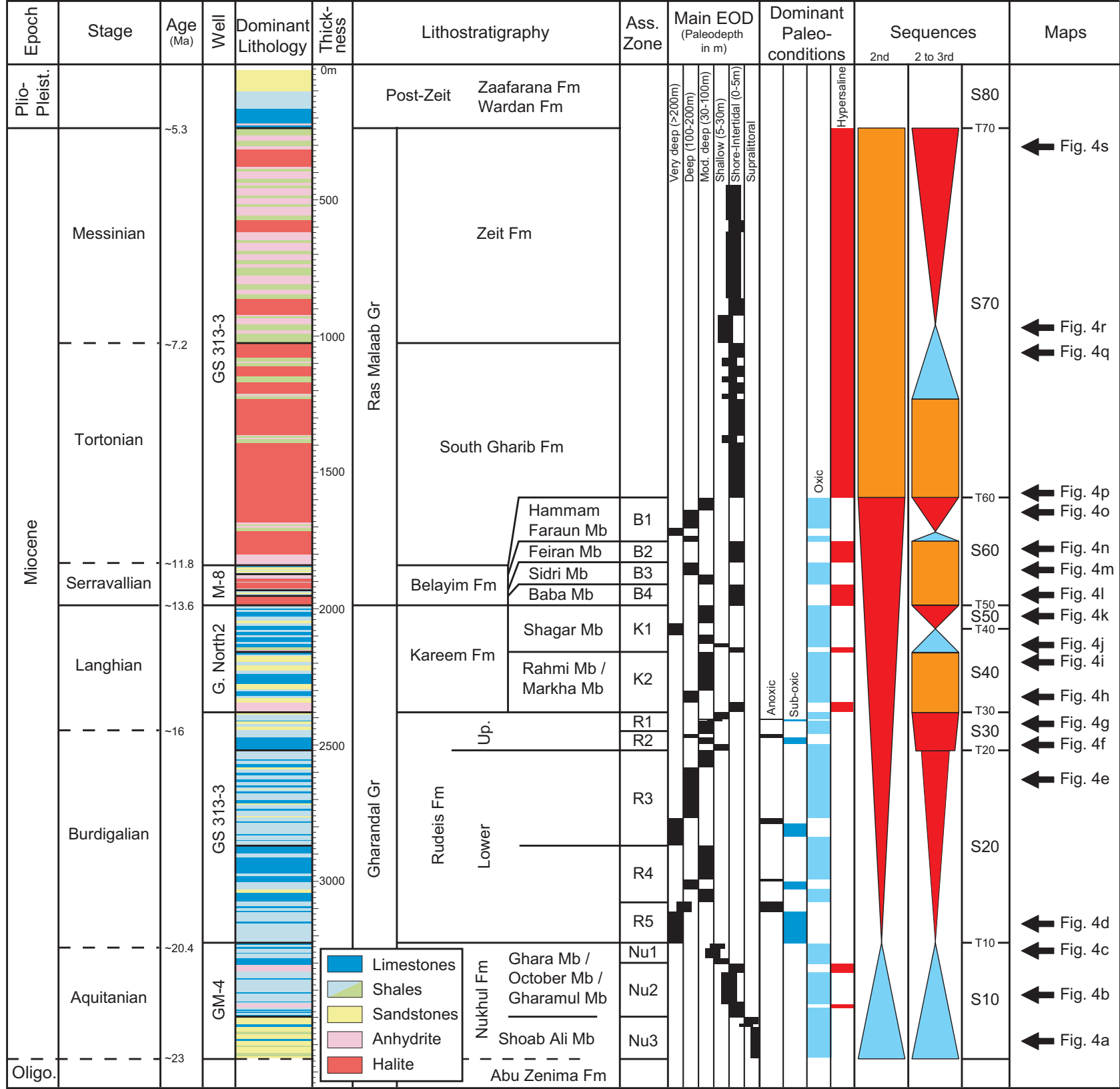


Figure 3

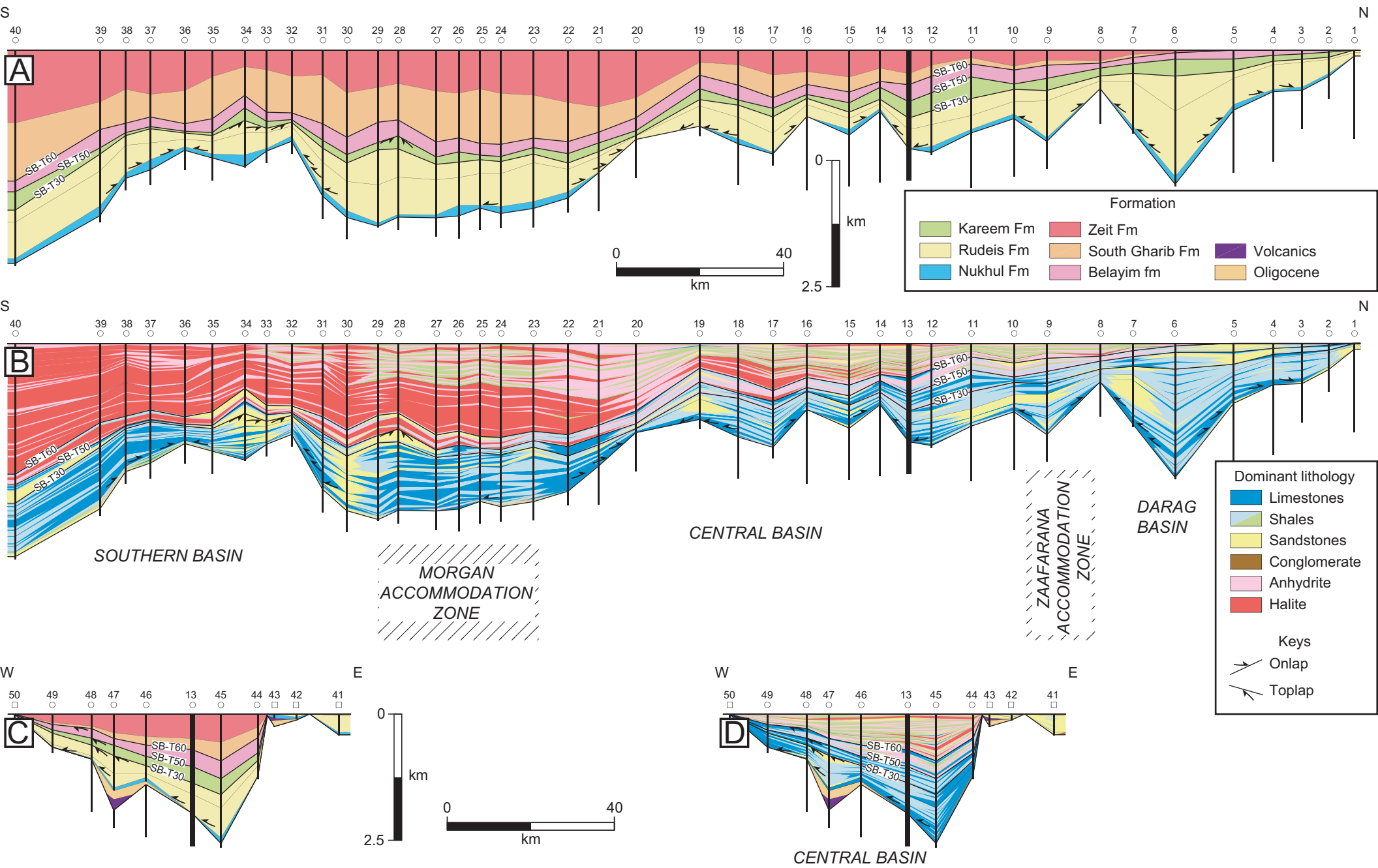


Figure4dg

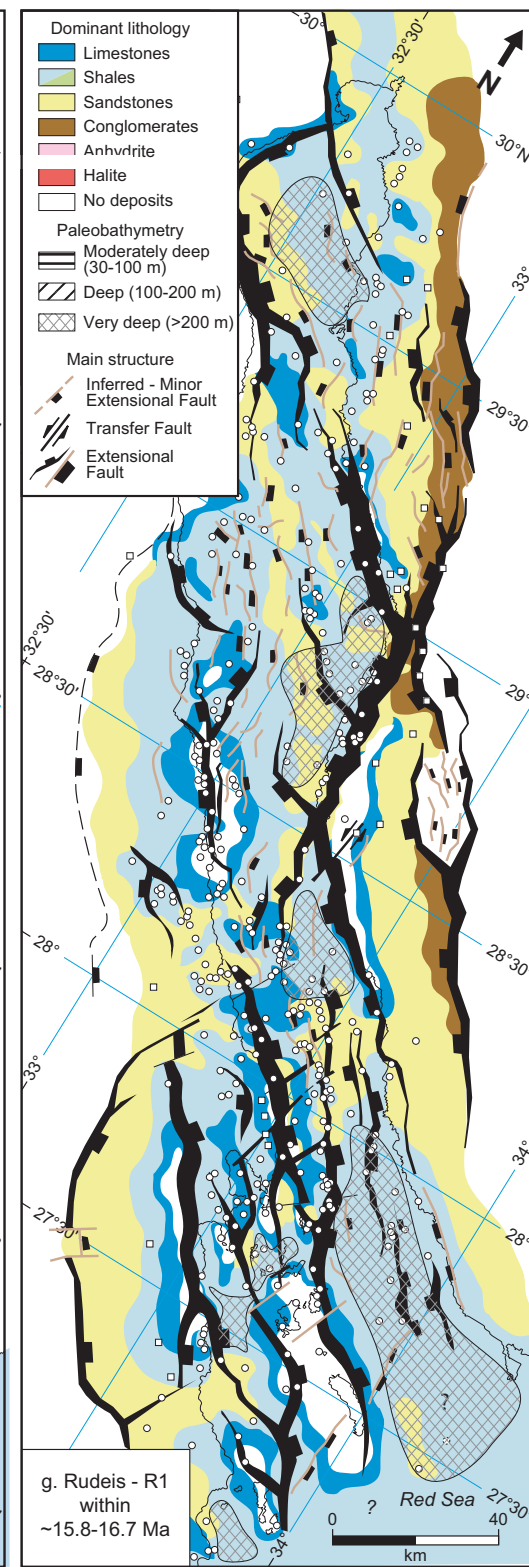
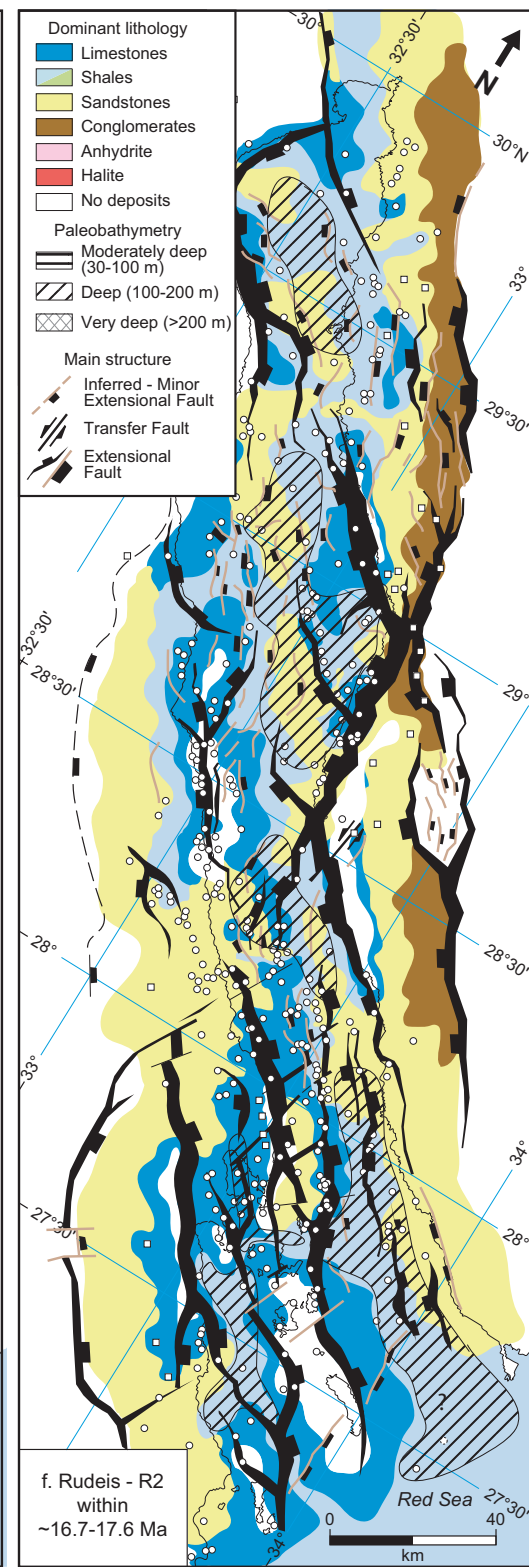
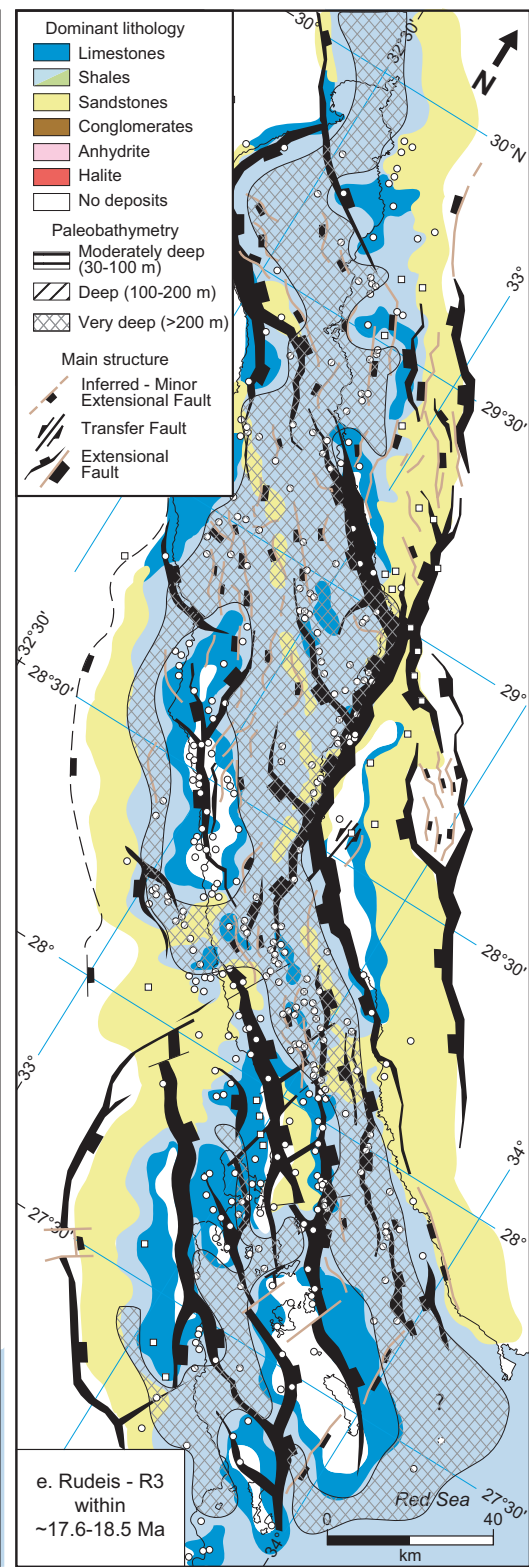
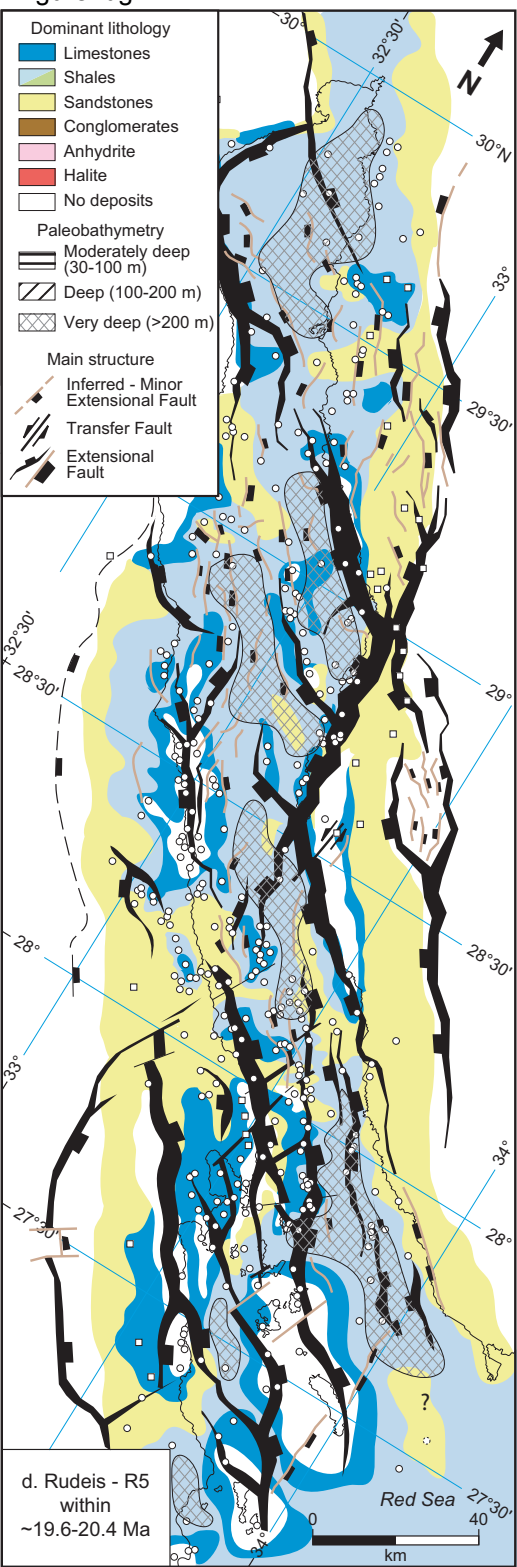


Figure 4hk

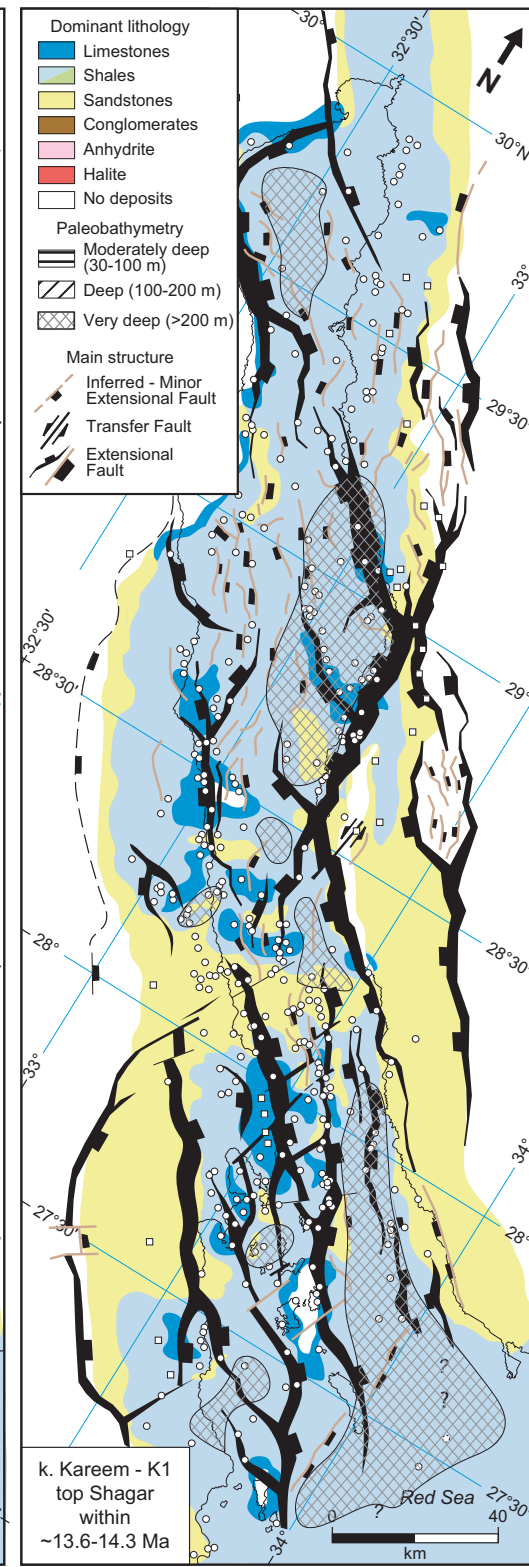
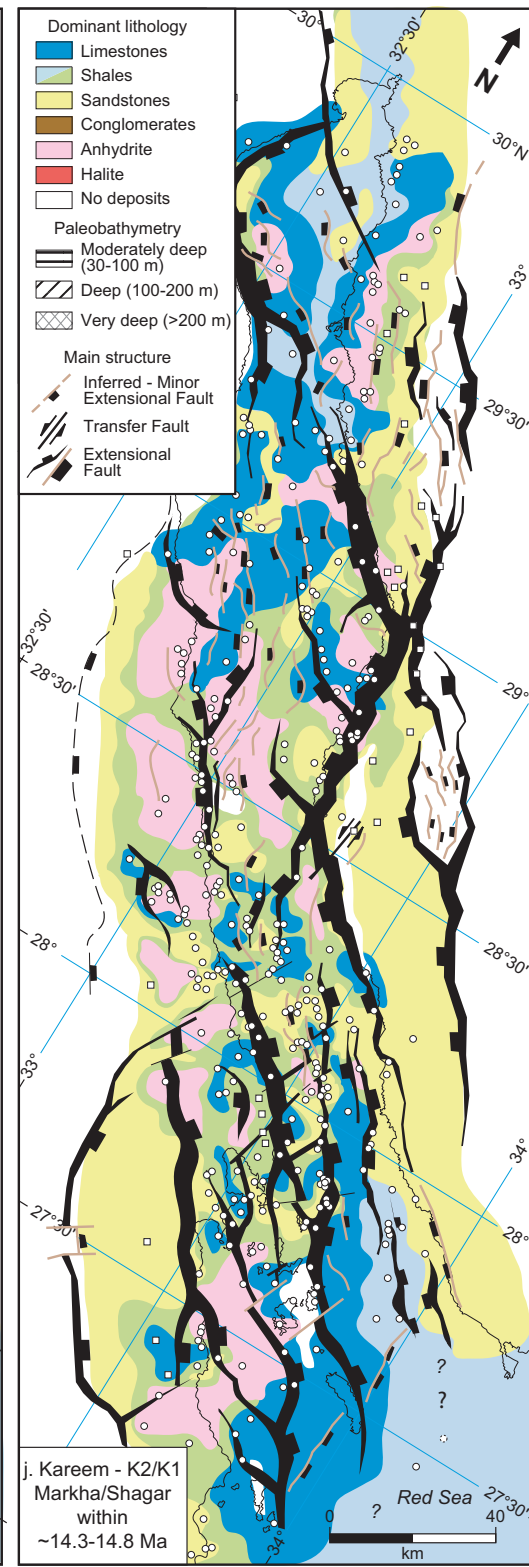
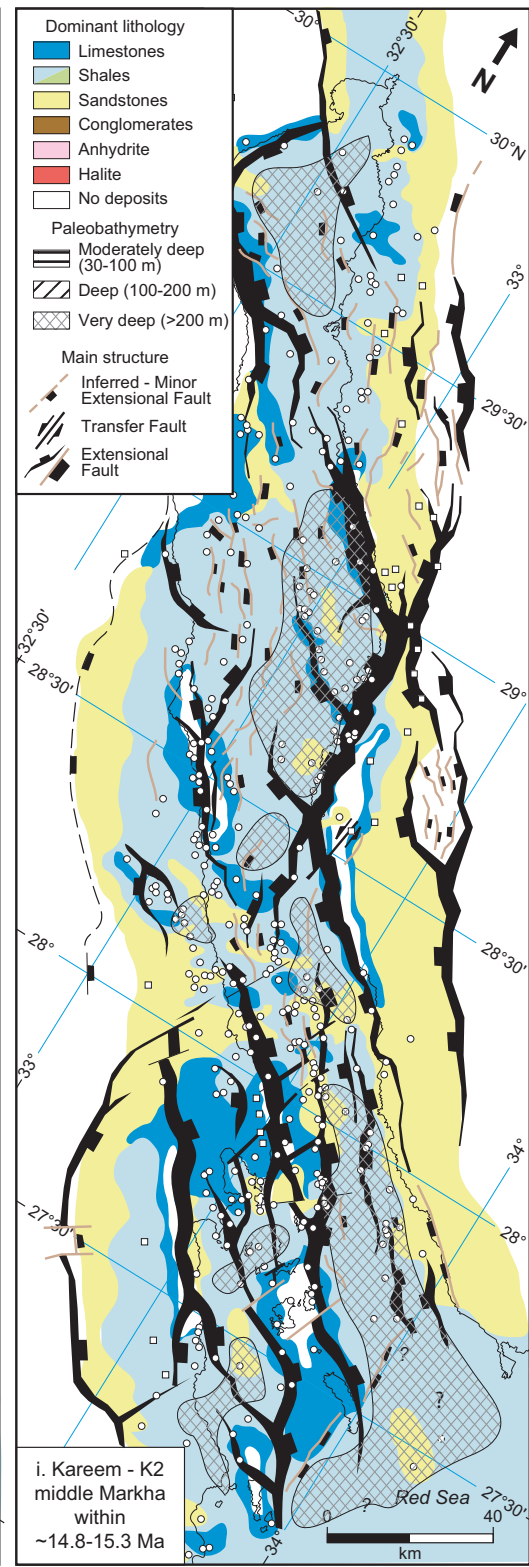
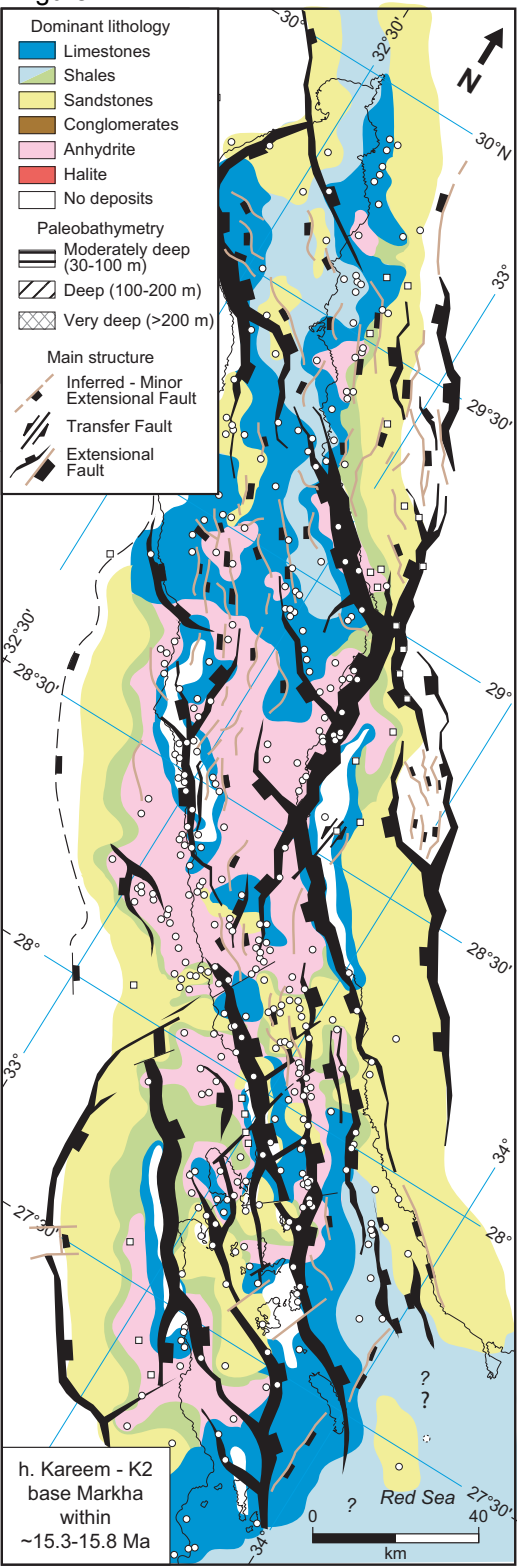


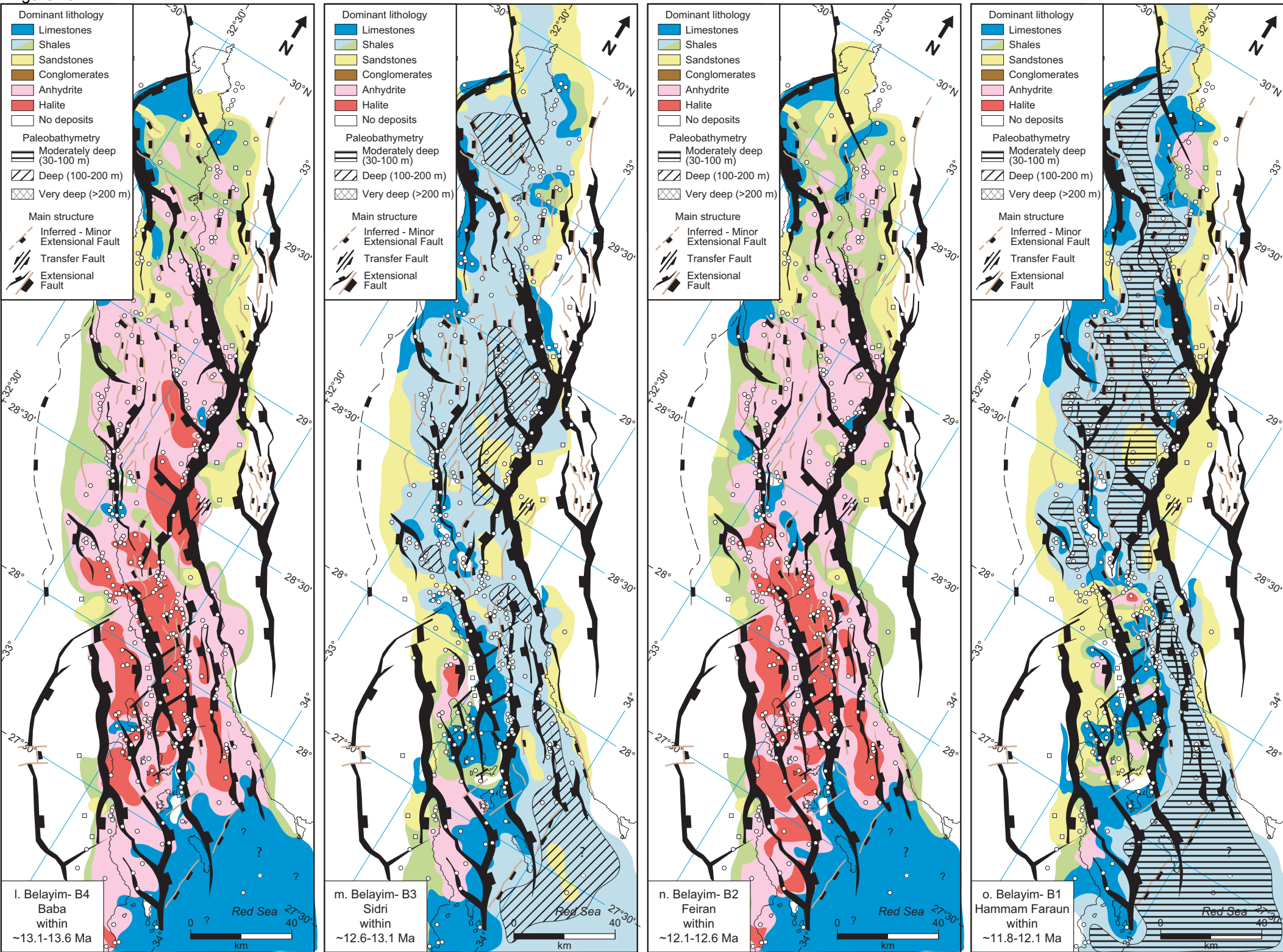
Figure 4

Figure 4ps

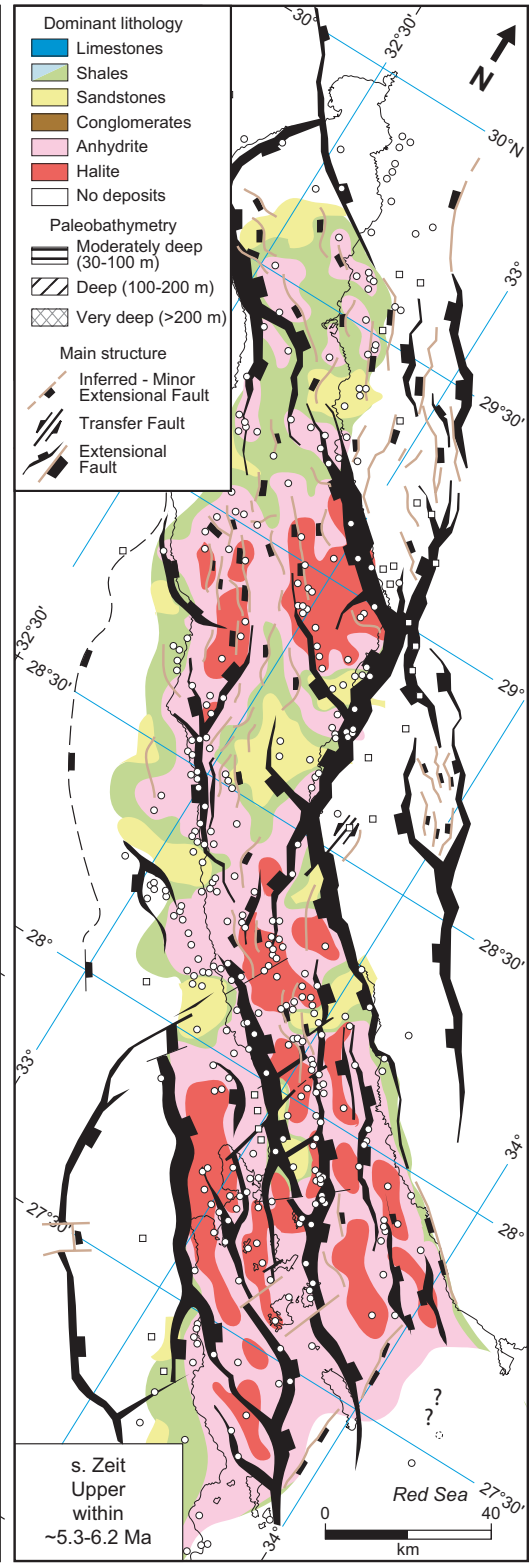
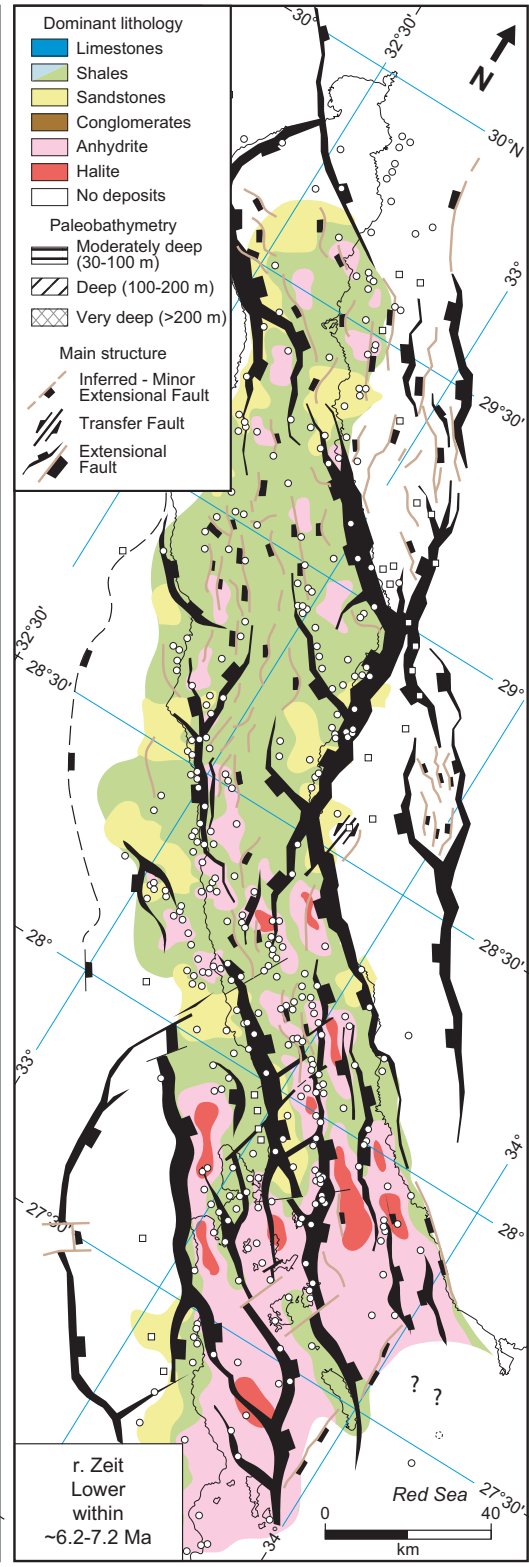
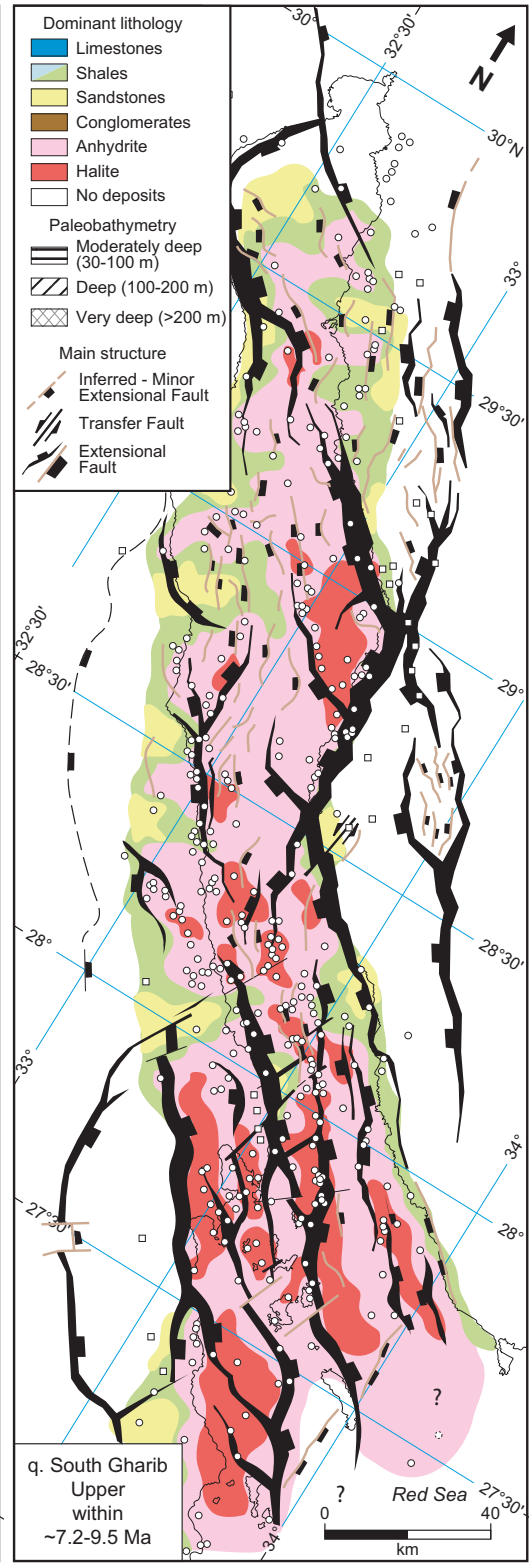
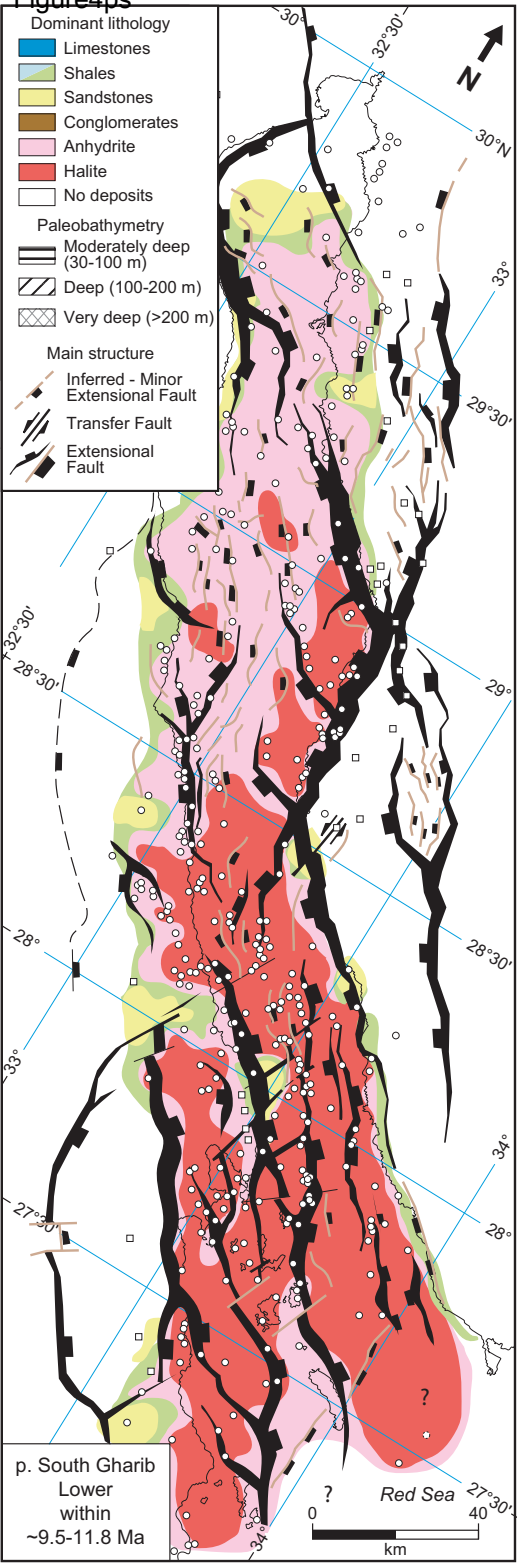


Figure5ad

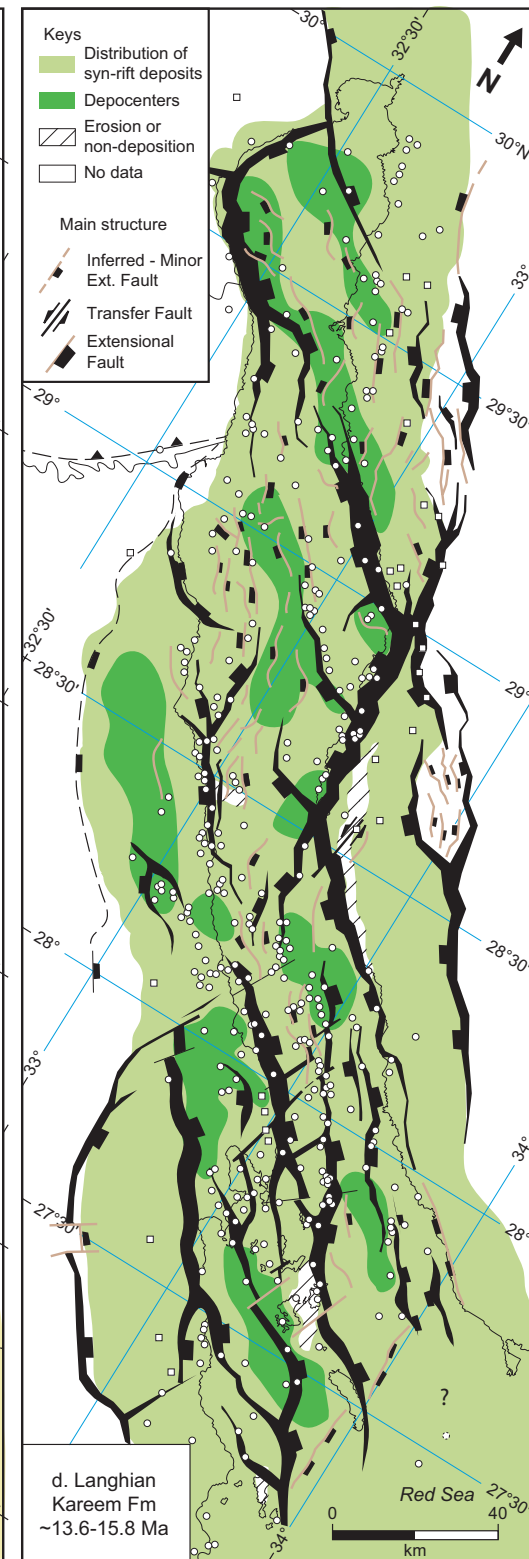
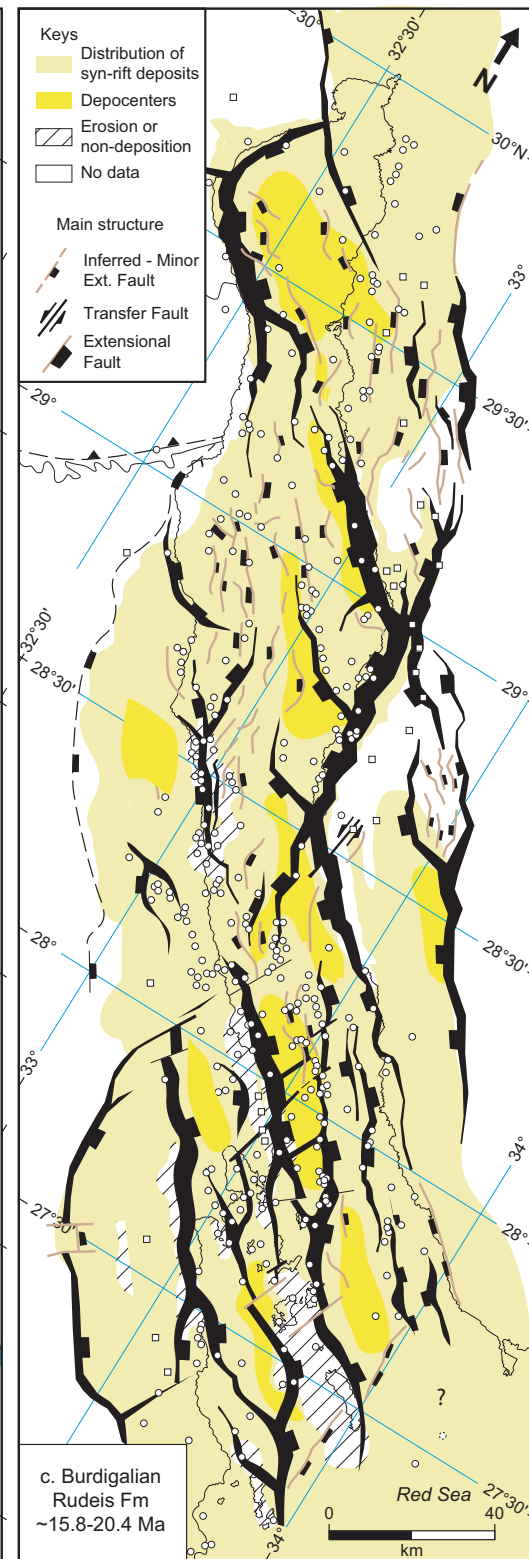
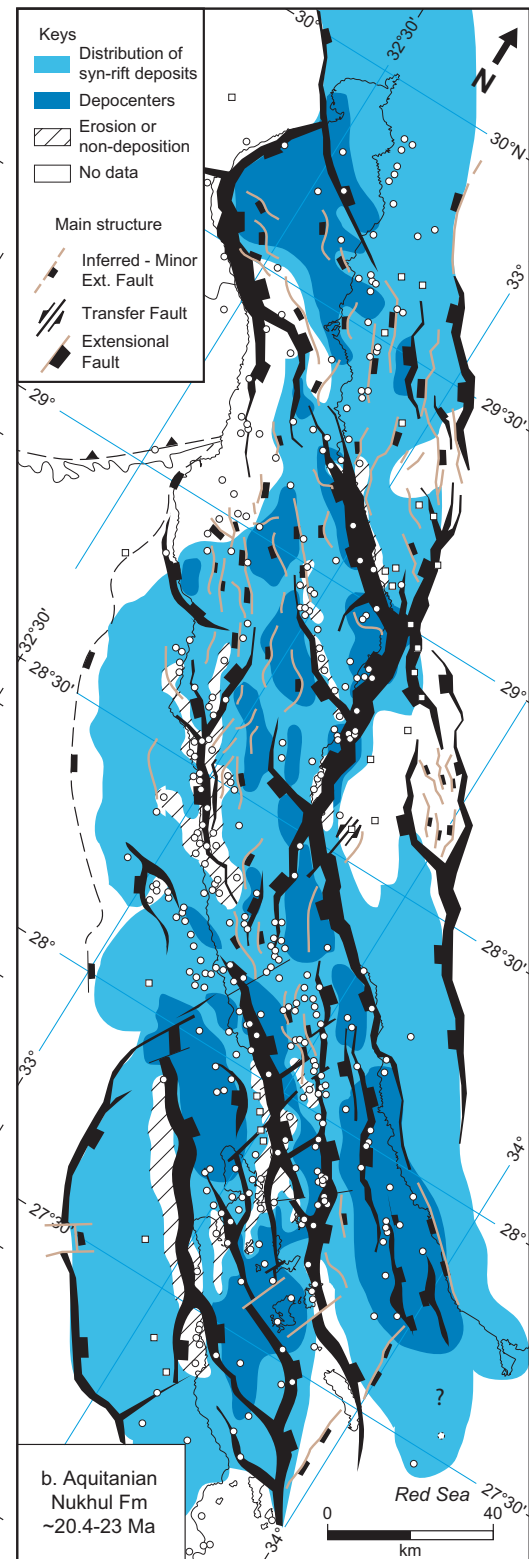
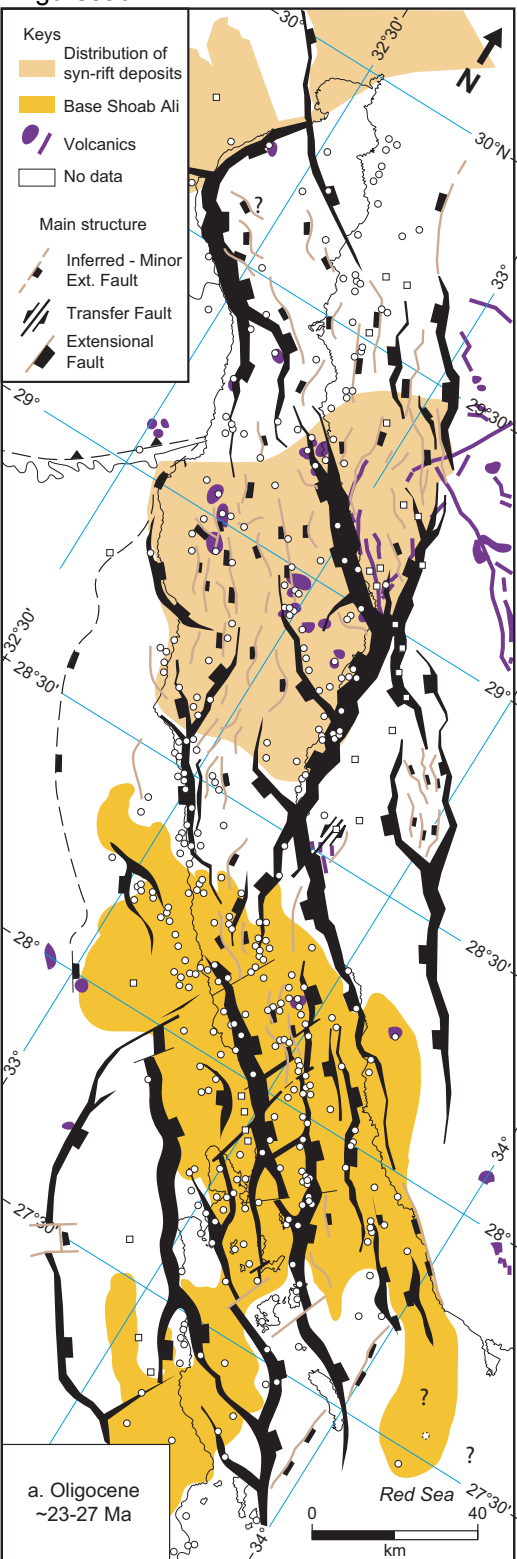


Figure5eg

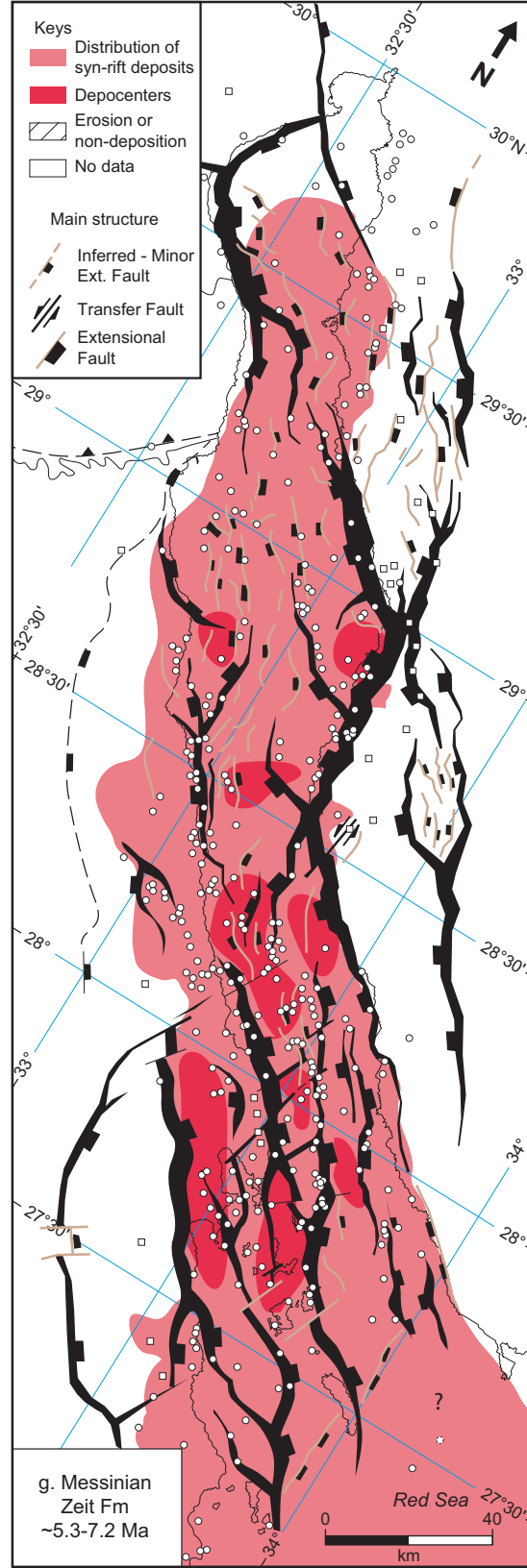
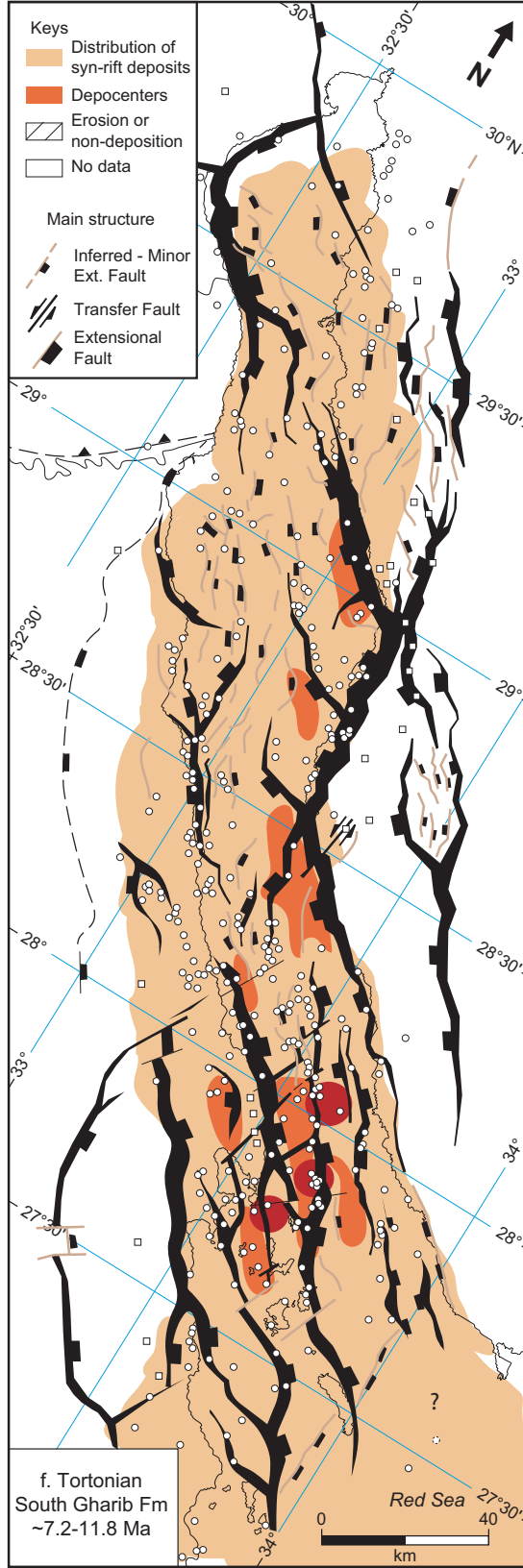
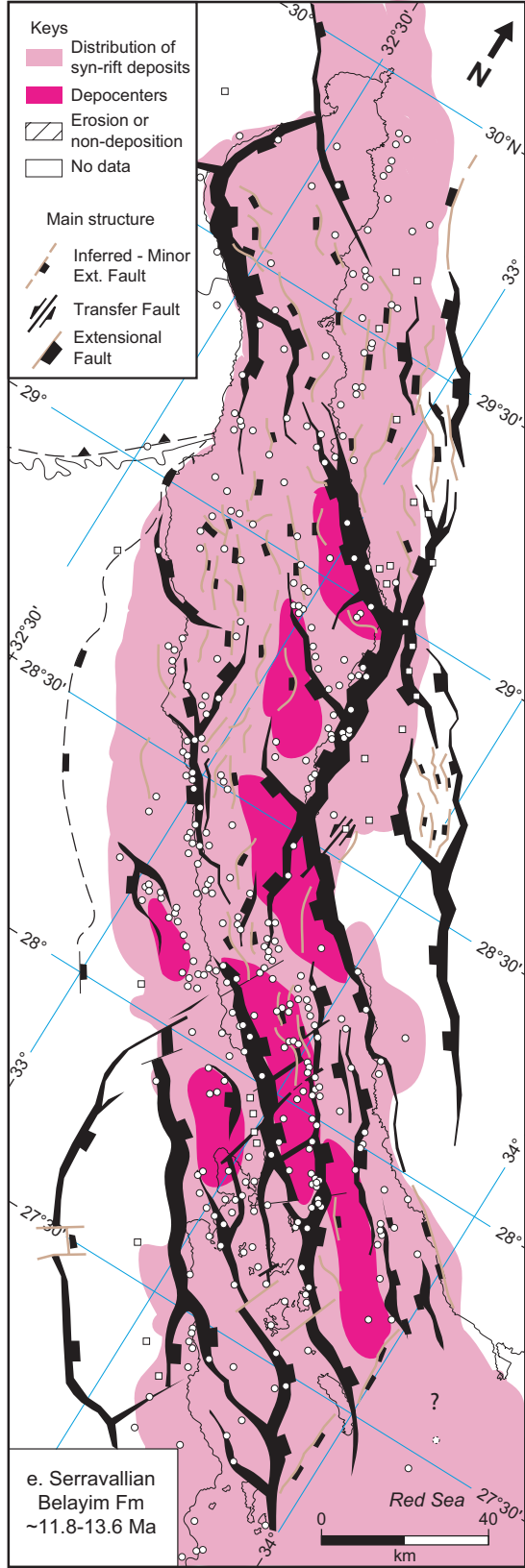


Figure6

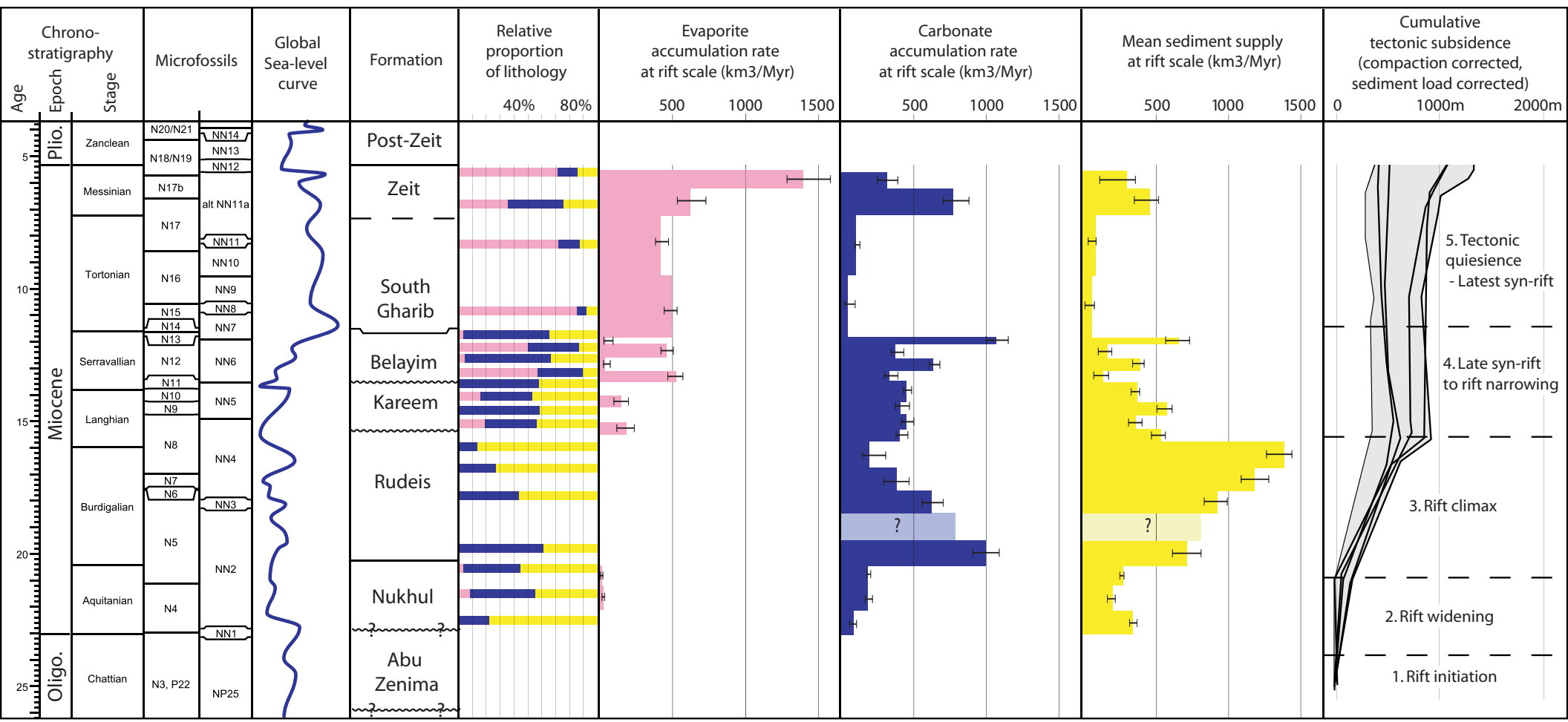


Table1

Formation	Map	Figure	Estimated duration (Myr)		Preserved Volume at rift scale		Relative proportion									Evaporite accumulation rate (km3/Myr)			Carbonate accumulation rate (km3/Myr)			Mean Sediment supply at rift scale (km3/Myr)		
			Age (Ma)	Duration (Myr)	Km3	Km3	Evaporites			Carbonates			Siliciclastics			Pref.	Max.	Min.	Pref.	Max.	Min.	Pref.	Max.	Min.
							Pref.	Max.	Min.	Pref.	Max.	Min.	Pref.	Max.	Min.									
Zeit	Zeit Upper	4s	5.3-6.2	0.9	3558	1779	0.71	0.8	0.65	0.15	0.18	0.11	0.15	0.18	0.11	1393.7	1581.3	1284.8	315.3	391.4	249.9	296.4	355.8	108.7
	Zeit Lower	4r	6.2-7.2	1		1779	0.35	0.41	0.30	0.39	0.45	0.36	0.25	0.29	0.20	624.0	729.4	533.7	772.6	880.6	703.0	452.6	515.9	347.2
South Gharib	South Gharib Upper	4q	7.2-9.5	2.3	2723	1361	0.71	0.8	0.65	0.15	0.2	0.15	0.13	0.14	0.09	421.4	473.5	384.7	99.8	130.2	96.5	79.8	82.9	27.6
	South Gharib Lower	4p	9.5-11.8	2.3		1361	0.84	0.9	0.75	0.07	0.15	0.04	0.09	0.12	0.01	497.6	532.7	443.9	47.0	97.7	25.6	51.5	71.0	5.5
Belayim	Belayim-B1 Hammam Faraun	4o	11.8-12.1	0.3	1874	469	0.03	0.06	0.02	0.62	0.67	0.58	0.35	0.39	0.30	44.7	93.7	31.2	1066.1	1151.0	998.7	657.4	730.9	564.8
	Belayim-B2 Feiran	4n	12.1-12.6	0.5		469	0.49	0.54	0.45	0.36	0.42	0.34	0.14	0.17	0.09	462.3	506.0	421.7	374.3	432.9	347.0	161.5	191.2	97.5
	Belayim-B3 Sidri	4m	12.6-13.1	0.5		469	0.04	0.08	0.03	0.62	0.66	0.59	0.34	0.37	0.30	38.5	75.0	28.1	634.3	680.3	607.0	386.2	416.1	336.1
	Belayim-B4 Baba	4l	13.1-13.6	0.5		469	0.56	0.61	0.50	0.32	0.38	0.29	0.12	0.15	0.06	525.4	571.6	468.5	333.6	391.7	298.2	130.1	168.7	66.7
Kareem	Kareem-K1 top Shagar	4k	13.6-14.3	0.7	1994	498				0.57	0.62	0.55	0.43	0.45	0.38				447.8	485.6	430.8	366.0	384.5	324.7
	Kareem-K2/K1 Markha/Shagar	4j	14.3-14.8	0.5		498	0.15	0.2	0.10	0.37	0.43	0.34	0.48	0.51	0.42	148.3	199.4	99.7	410.2	471.5	374.2	570.8	610.1	503.9
	Kareem-K2 middle Markha	4i	14.8-15.3	0.7		498				0.58	0.64	0.53	0.42	0.47	0.36				451.6	501.3	415.1	361.9	401.6	307.6
	Kareem-K2 base Markha	4h	15.3-15.8	0.5		498	0.18	0.24	0.12	0.37	0.42	0.35	0.44	0.47	0.40	184.2	239.3	119.6	406.0	460.6	378.6	532.3	562.3	466.2
Rudeis	Rudeis-R1	4g	15.8-16.7	0.9	5999	1200				0.15	0.21	0.10	0.85	0.9	0.79				193.9	308.0	146.6	1388.4	1439.8	1263.9
	Rudeis-R2	4f	16.7-17.6	0.9		1200				0.26	0.32	0.20	0.74	0.8	0.68				385.0	469.3	293.3	1180.0	1279.9	1087.9
	Rudeis-R3	4e	17.6-18.5	0.9		1200				0.43	0.48	0.38	0.57	0.62	0.52				624.1	703.9	557.3	919.2	991.9	831.9
	Rudeis-R5	4d	19.6-20.4	0.8		1200				0.61	0.66	0.55	0.39	0.45	0.34				998.3	1088.9	907.4	711.0	809.9	611.9
Nukhul	Nukhul-Nu1	4c	20.4-21.2	0.8	969	323	0.03	0.06	0.02	0.41	0.46	0.40	0.56	0.57	0.51	11.8	24.2	8.1	183.0	204.3	178.0	270.6	276.2	247.4
	Nukhul-Nu2	4b	21.2-22.1	0.9		323	0.08	0.1	0.05	0.47	0.55	0.42	0.45	0.5	0.37	27.8	35.9	17.9	184.9	217.1	166.9	195.7	215.3	160.5
	Nukhul-Nu3 top Shoab Ali Mb.	4a	22.1-23	0.9		323				0.22	0.27	0.15	0.78	0.85	0.73				85.2	106.6	59.2	337.7	366.1	314.4